Nuclear Polarization and Charge Parameters Using the Muonic 2s State*

P. Martin,† G. H. Miller,‡ and R. E. Welsh
College of William and Mary, Williamsburg, Virginia 23185

D. A. Jenkins and R. J. Powers§
Virginia Polytechnic Institute and State University, Blacksburg, Virginia 24061

A. R. Kunselman
University of Wyoming, Laramie, Wyoming 82070

(Received 2 October 1972; revised manuscript received 13 August 1973)

Muonic x-ray transition energies have been measured in ^{120}Sn, ^{138}Ba, ^{140}Ce, ^{142}Ce, and ^{206}Pb using a high-efficiency Ge(Li) detector. Precise measurements and relative-intensity measurements have made it possible to identify transitions to and from the 2s state in each of these targets. There is good agreement between theoretical and experimental relative intensities for these transitions, except for the ^{206}Pb nucleus. These transition energies, together with those from the $2p$-$1s$, $3d$-$2p$, and $4d$-$2p$ transitions are used to deduce sets of nuclear charge parameters. It has been found that for each target except ^{120}Sn, the best agreement between theory and experiment is obtained by applying the theoretical nuclear polarization corrections to all levels with $n > 1$, and varying the nuclear polarization induced by the muon in the $1s$ state. The nuclear polarization values determined were 5.8 ± 1.5 keV for ^{120}Sn, 6.7 ± 1.4 keV for ^{138}Ba, 6.5 ± 1.3 keV for ^{140}Ce, 7.0 ± 1.4 keV for ^{142}Ce, and 5.5 ± 1.7 keV for ^{206}Pb. These results are in fair agreement with the most recent theoretical predictions.

1. INTRODUCTION

The idea that muonic x rays would be a useful tool for measuring nuclear charge parameters was originally suggested by Wheeler[1,2] and was extended by Hill and Ford.[3] Hill and Ford also attempted to fit the experimental data to both uniform- and nonuniform charge distributions. They pointed out that the $3d$-$2p$ and $2s$-$2p$ transitions were highly sensitive to the shape of the nuclear charge distribution and should be used, together with the $2p$-$1s$ transitions, to determine nuclear charge parameters.

The present set of experiments was designed to make accurate energy measurements of transitions to and from the muonic $2s$ state, as well as the more easily observed transitions, over a range of Z. These sets of transition energies were used to derive parameters for the nuclear charge distribution, and to investigate whether better agreement could be obtained between theoretical and experimental energies by accounting for the effects of nuclear polarization by the muon.

When a muon approaches a nucleus it is possible for the electrostatic interaction to excite the nucleus into virtual states, and the effect is observed as a small change in the atomic transition energies. This is known as nuclear polarization and recent theoretical evaluations[4-6] have given predictions between 3 and 6 keV for the effect produced by a muon in the $1s$ atomic state of the elements studied here. The effect increases with increasing Z, and increases the binding energy of the state.

The $1s$, $2p$, and $2s$ muonic states all have strong dependence upon the parameters used to describe the charge distribution, so that in principle one can extract two charge parameters and the nuclear polarization from experimental data involving these states. With the use of high-resolution Ge(Li) detectors, it is not difficult to determine muonic transitions to within 0.25 keV, so that the validity of effects several times this magnitude are extremely important, and will produce a considerable variation in the other parameters used to describe the charge distribution. The evaluation of the transition energies is also important as a check of the theoretical calculations of nuclear polarization.

Excellent reviews of the progress of muonic atoms are given in the articles by West,[7] Devons and Duerdoth,[8] Wu and Wilets,[9] and Scheck and Hüfner.[10] The latter two are the most comprehensive in their discussion of the effects of nuclear polarization in muonic atoms. The first reported observations of transitions involving the $2s$ state were by Kessler *et al.* and Anderson *et al.*[11] Anderson *et al.* derived a value for the $1s$ nuclear polarization in ^{206}Pb but did not apply corrections to any of the higher levels. We later observed and reported transitions[12] involving the $2s$ state in ^{140}Ce [Ref. 12(a)] and ^{208}Pb [Ref. 12(b)],

as has CERN for Tl (Ref. 13).

Section 2 is a summary of the importance of the $2s$ level and the theory underlying the evaluation of the transition energies. The experimental and theoretical techniques are described in Sec. 3. The results and their interpretation are given in Sec. 4. Section 5 contains the conclusions which were drawn from the data, together with the limitations which we placed on the analysis, and possible future improvements for this type of experiment.

2. THEORY

The muon energy levels and eigenfunctions were obtained by numerically solving the Dirac equation using the methods of McKee.[14] The only muonic levels exhibiting measurable finite-size effects are the $1s$, $2s$, $3s$, $2p$, and $3p$ levels. The energies of the other levels are experimentally indistinguishable from those for a point nuclear charge. This is demonstrated in Fig. 1 where the muon linear probability densities ($r^2 \times$ wave-function probability density) are plotted as a function of radial distance from the center of the nucleus, for the various levels in ^{138}Ba. A typical charge distribution has been superimposed to demonstrate the overlap of the nucleus and the wave functions.

In general each level is sensitive to a different moment of the nuclear charge distribution,[15] and at most, the number of deducible parameters will be the number of distinct levels that have been measured experimentally. In this context each member of a fine-structure doublet has the same functional dependence, because of the similarity of their linear probability densities (Fig. 1). If a conventional Fermi function is used to describe the charge distribution,

$$\rho(r) = \rho_0[1 - \exp(r - c)/t]^{-1} , \quad (1)$$

the energies of the $1s$ and $2p$ levels can be used to derive the parameters c and t. In order to ask meaningful questions about a third nuclear parameter it is essential to determine the energy of other levels to an experimental uncertainty which is only a small percentage of the finite-size effect. Because of their large finite-size effect, the $2s$ and $3p$ levels were used in this analysis.

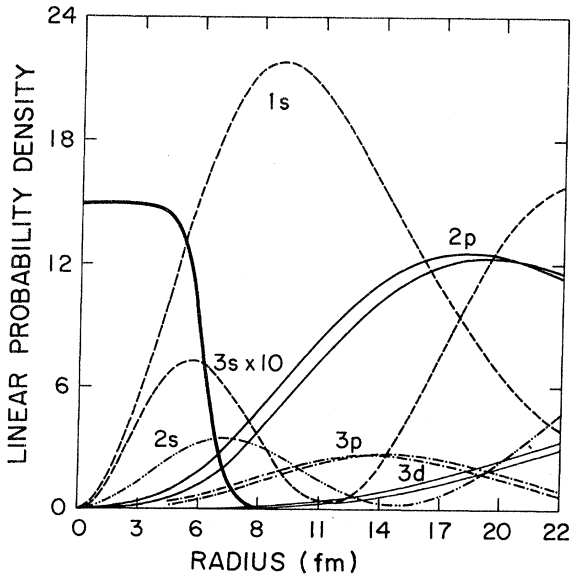

FIG. 1. The linear probability density ($r^2 \times$ wave-function probability density) for various levels in ^{138}Ba. The units are arbitrary, and the charge distribution is superimposed.

All transitions affected by the finite size of the nucleus exhibit strongest dependence on the parameter c of the charge distribution. Scheck and Hüfner[10] have determined the dependence of the principal transitions on a nuclear parameter orthogonal to $\langle r^2 \rangle$. They show $\langle r^2 \rangle$ to be a function of both c and t. Excluding $2p$-$1s$ transitions they find that the $2s$-$2p$ doublet and the $3p$-$2s$ doublet are the most valuable transitions for determining parameters other than $\langle r^2 \rangle$. The muonic $2s$ level has not been used in charge determinations until recently,[11-13] because of the difficulty of observing transitions involving it. Using a cascade calculation for ^{140}Ce, it is predicted that at most $3\frac{1}{2}\%$ of all captured muons will pass through the $3p$ state, and about only $1\frac{1}{2}\%$ will pass through the $2s$ state. Because the selection rules for Auger transitions and electric dipole transitions favor $\Delta l = \pm 1$, the outer "circular" orbits ($l = n - 1$) become preferentially populated and the dominant transitions for $n \leq 6$ are between successive circular orbits.[16] The most intense transitions are the $2p$-$1s$ doublet (87%), the $3d$-$2p$ triplet (80%), and the $4f$-$3d$ triplet (71%). Table I shows the percentage of muons predicted to pass through each state with $n \leq 4$ for ^{140}Ce, assuming a statistical distribution in the $n = 14$ level.

The solution of the Dirac equation requires the use of some empirical form for the charge distributions. From the beginning of muonic x-ray work the question of which functional form to use for the charge distribution has been of considerable interest. The earliest calculations used a uniform spherical charge distribution.[1,17,18] The idea of using a slightly more physical model, with no amplitude discontinuity was initially investigated by Hill and Ford[3] using a series of modified Gaussian and modified exponential functions. Hill and Ford concluded that there was no unique distribution and that many forms could give acceptable results. Ford and Wills have since discussed

TABLE I. Relative intensities and level populations for all states with $n<4$ in ^{140}Ce. Numbers represent the percentage of all captured muons making the given transition, accounting for electric dipole, electric quadrupole, and Auger emission. An omitted entry implies no transition allowed or a transition probability <0.01.

Initial state	Population (%)	Final state $3s_{1/2}$	$3p_{3/2}$	$3p_{1/2}$	$3d_{5/2}$	$3d_{3/2}$	$2s_{1/2}$	$2p_{3/2}$	$2p_{1/2}$	$1s_{1/2}$
$n>4$		0.21	1.55	0.76	9.33	6.28	0.21	3.70	1.88	1.99
$4f_{7/2}$	35.91		0.05		35.33			0.54		
$4f_{5/2}$	27.01			0.03	1.69	24.88		0.09	0.32	
$4d_{5/2}$	5.64		1.4					4.0		0.18
$4d_{3/2}$	3.8		0.16	0.78				0.4	2.3	0.1
$4p_{3/2}$	0.7	0.07					0.14			0.5
$4p_{1/2}$	0.37	0.04					0.08			0.24
$4s_{1/2}$	0.16		0.09					0.07		
$3s_{1/2}$	0.37		0.2	0.15				0.02		
$3d_{5/2}$	46.4						0.04	45.0		1.3
$3d_{3/2}$	31.2						0.02	4.7	25.6	0.8
$3p_{3/2}$	3.5						0.8			2.6
$3p_{1/2}$	1.6						0.45			1.15
$2s_{1/2}$	2.1							1.2	0.9	
$2p_{3/2}$	59.7									59.7
$2p_{1/2}$	31.2									31.2

extensively the matching of experimental results with various functional forms of the charge distribution.[19,20] They have shown that each transition is sensitive to a unique moment $\langle r^{\alpha}\rangle$ of the charge distribution.[15] The value of α is found to be essentially model-independent, and approximately a linear function of Z, with the zero intercept being an integral value. Their approach did not show a unique moment $\langle r^{\alpha}\rangle$ for the $2s$-$2p_{1/2}$ transitions. Wu and Wilets[9] explain this discrepancy by expanding the potential generated by the muon, as a power series in the distance from the muon, over the region of the nucleus, retaining only the most significant term. The behavior of the $2s$ level suggests that this is not a good approximation for the muonic potential over the nucleus. In an attempt to eliminate the slight functional dependence of the method of Ford and Wills,[15] Barrett[21] has used a more general form for the functional expansion. This method can be adjusted to give consistent energies over a wider range of functions than is possible using the form of Ford and Wills.

All the functions so far described have the common disadvantage of having no direct physical derivation. Their use is justified by their convenience and by their giving satisfactory agreement with experiment. If the shell structure of the nucleus were well known, it would be possible to synthesize a charge distribution by summing the respective proton wave functions. The first attempts to derive a charge distribution by this method were carried out by Perey and Schiffer[22] and Elton and Swift.[23]

Elton, Webb, and Barrett[24] have recalculated the charge distribution using single-particle wave functions in an energy-independent nonlocal potential. This approach yields excellent agreement with shell separation energies but produces a charge distribution for ^{208}Pb which is in conflict with the analysis of electron-scattering experiments.[25] Another approach which may provide realistic charge distributions is that due to Vautherin and Brink.[26]

For the future it may be possible to relate muonic transition energies to internucleon forces via the Vautherin-Brink theory, or a charge distribution may be specified by a set of moments rather than by the familiar nuclear parameters. The present development of the latter seems inappropriate for these data, since it appears unable to describe adequately transitions involving the muonic $2s$ state, which is the real strength of these experimental results.

Because of the indicated theoretical problems, the data were analyzed in terms of a generalized Fermi distribution, which has four variable parameters corresponding to a radius c, a skin thickness t, a fall-off parameter m, and a central depression w. It is expressed mathematically as

$$\rho(r,c,n,w,m)=\rho_0\frac{1+wr^2/c^2}{1+\exp\{n^m[(r/c)^m-1]\}}\,, \qquad (2)$$

where ρ_0 is a normalization constant and is evaluated numerically by requiring

$$4\pi\int\rho(r,c,n,w,m)r^2\,dr=Ze \qquad (3)$$

TABLE II. Total vacuum polarization effect (in keV). This effect increases the binding energy.

Level	^{120}Sn	^{138}Ba	^{140}Ce	^{142}Ce	^{206}Pb
$1s_{1/2}$	35.89	42.07	44.22	44.07	67.02
$2s_{1/2}$	7.82	9.72	10.40	10.37	19.36
$2p_{1/2}$	10.53	13.90	15.12	15.13	32.30
$2p_{3/2}$	9.81	12.87	13.97	13.99	29.73
$3p_{1/2}$	3.32	4.43	4.84	4.84	10.81
$3p_{3/2}$	3.14	4.19	4.57	4.58	10.28
$3d_{3/2}$	2.68	3.74	4.12	4.12	10.55
$3d_{5/2}$	2.60	3.54	3.89	3.90	9.89
$4d_{3/2}$	1.11	1.54	1.70	1.71	4.62
$4d_{5/2}$	1.08	1.49	1.64	1.65	4.38
$4f_{5/2}$	0.89	1.25	1.38	1.39	3.71
$4f_{7/2}$	0.88	1.23	1.36	1.36	3.61

and

$$n=\frac{4c}{t}\ln 3 \ .$$

A. Corrections to Energy Levels

The muon energy levels were evaluated by numerically solving the Dirac equation. Each energy eigenvalue was then corrected for radiative effects. The vacuum polarization potential was calculated to the first order using the methods of Schwinger[27] and added to the Coulomb potential when solving the Dirac equation. Higher-order effects were included from the calculations of Blomquist.[28] The electron screening corrections using the Vogel[29] technique and the relativistic center-of-mass corrections presented by Fricke[30] were included. The sum of the vacuum-polarization effects for each important level in each nucleus is shown in Table II. This effect is between 0.5 and 1% of the energy eigenvalue and is by far the largest correction. Higher-order effects account for ~1% of the total vacuum-polarization correction. Recent high-resolution work[31,32] has detected a small energy discrepancy beyond the sensitivity of this experiment which cannot be explained with current theory.

The effect of the Lamb shift and the anomalous magnetic moment of the muon were calculated following the methods of Barrett *et al.*[33] and are shown in Table III. The Lamb shift accounts for ~80% of these values and is estimated to be accurate to within 30%. This uncertainty in the 1*s* level is twice the experimental energy uncertainties and is a possible source of error in the nuclear charge parameter calculations. When more accurate values of the Lamb shift are available the nuclear parameters should be recalculated.

The third effect allowed for was nuclear polarization. Nuclear polarization is produced by the muon-nucleus electrostatic interaction. Because of the penetration of the nucleus by the muon, the eigenfunctions of the original system are perturbed and there is an associated change in the energy eigenvalues. In mathematical terms this appears through second-order perturbation theory, and can be thought of as the electrostatic interaction mutually exciting the nucleus and the muon into virtual intermediate states.

The earliest discussion of nuclear polarization was by Breit, Arfken, and Clendenin[34] in 1950. The effect was expected to be much more important in muonic atom studies than in electronic atoms because of the larger nuclear overlap by the muon. Cooper and Henley[18] calculated the nuclear polarization for the Fitch and Rainwater results[35] on ^{208}Pb, and deduced an upper limit of 60 keV for the 1*s* state.

The methods for calculating nuclear polarization have been considerably refined and recent calculations[4-6] predict a value of ~6 keV for the nuclear polarization of ^{208}Pb by a muon in the 1*s* state.

Although the nuclear polarization by the muon in the 1*s* state is principally treated as a variable

TABLE III. Energy corrections for the Lamb shift and the anomalous magnetic moment. The energies are in keV, and a negative sign decreases the binding energy of the state.

Level	^{120}Sn	^{138}Ba	^{140}Ce	^{142}Ce	^{206}Pb
$1s_{1/2}$	−1.80	−2.05	−2.14	−2.11	−2.76
$2s_{1/2}$	−0.39	−0.46	−0.48	−0.48	−0.70
$2p_{1/2}$	−0.03	−0.07	−0.08	−0.08	−0.35
$2p_{3/2}$	−0.10	−0.17	−0.19	−0.20	−0.65
$3p_{1/2}$	−0.02	−0.03	−0.05	−0.04	−0.18
$3p_{3/2}$	−0.04	−0.07	−0.07	−0.07	−0.26
$3d_{3/2}$	0	+0.01	+0.02	+0.01	+0.04
$3d_{5/2}$	0	−0.01	−0.01	−0.01	−0.05

TABLE IV. Theoretical nuclear polarization values (in keV) with errors in parentheses. With the exception of the 3*d* level in ^{206}Pb these increase the binding energy of the levels.

Level	^{120}Sn [a]	^{138}Ba [a]	^{140,142}Ce [a]	^{206}Pb [a]	^{206}Pb [b]
$1s_{1/2}$	2.7	3.4	3.6	6.0(0.6)	6.8(2.0)
$2s_{1/2}$	0.67	0.7	0.8	1.2(0.2)	1.6(0.7)
$2p_{1/2}$	0.33	0.5	0.6	1.9(0.2)	1.9(0.3)
$2p_{3/2}$	0.33	0.5	0.6	1.9(0.2)	1.8(0.3)
$3p_{1/2}$	...	...	...	...	0.7(0.2)
$3p_{3/2}$	...	...	...	...	0.7(0.2)
$3d_{3/2}$	...	...	...	...	−0.03(0.02)
$3d_{5/2}$	...	...	...	...	0

[a] References 5 and 9.
[b] Reference 6 as calculated for ^{208}Pb.

TABLE V. Chemical composition and physical properties of the targets.

Target	^{120}Sn	^{138}Ba	^{140}Ce	^{142}Ce	^{206}Pb
Dimensions (cm)	17×8×0.5	15×7.5×1.3	15×15×1.3	7.5×7.5×1.3	14×12×1
Total mass (g)	165	185.6	694.6	108	1650
Chemical form	SnO_2	$Ba(NO_3)_2$	CeO_2	CeO_2	Radiogenic
Isotopic composition	120 98.6%	138 97.2%	140 99.7%	142 92.8%	206 88.0%
	118 0.5%	137 1.8%	142 0.3%	140 7.2%	207 9.0%
	119 0.4%	136 0.9%			208 3.0%

parameter it is necessary to account for the effects from the other levels if they are comparable with the experimental energy uncertainties. Detailed calculations have been made by Chen[5] of the effects of nuclear polarizations by the $2s$ and $2p$ levels for several Z, and the results are shown in Table IV. These values were taken from the figures in Ref. 9. Calculations have also been made for ^{208}Pb by Skardhamar[6] using a different theoretical model, and are in excellent agreement with those of Chen. Predictions by Tanabe[36] for the higher levels ($n \geq 3$) are too small to be of importance for these experimental results and do not agree with the predictions of Skardhamar. All of the values used were larger than the energy uncertainties so that any parameter calculation which allows for a nuclear polarization effect from the $1s$ level must also account for the effects in the higher levels. Chen estimates an uncertainty in the $1s$ and $2s$ levels of about 30% because of a lack of knowledge of the monopole modes of nuclear excitation, except for lead where the uncertainty is 10%. The effect of monopole excitation modes is very much smaller for the other levels and he expects their uncertainties to be correspondingly smaller. The uncertainties in the charge-parameter determinations reflect not only the experimental errors but also the theoretical uncertainties in the Lamb shift and nuclear polarization calculations.

3. EXPERIMENTAL PROCEDURE AND DATA ANALYSIS

The data for this experiment were collected during four experimental periods using the meson channel at the National Aeronautics and Space Administration Space Radiation Effects Laboratory in Newport News, Virginia. A complete description of the experimental apparatus, the electronics, the data collection techniques, and the data analysis is given in Ref. 12(b). The only differences between this experiment and the one described in Ref. 12(b) were the composition of the targets and the calibration sources used. Table V shows the chemical composition of the targets, their dimensions, and their masses. All the targets were in powder form except the ^{206}Pb which was a solid sheet. The powder was made into a target by encapsulating it in a rectangular box made from a thin plastic sheet.

A complete list of the calibration sources together with their uses is given in Table VI. The system linearity was determined using the sources, a precision pulser, and the 511-keV energy difference between the full-energy, single-escape, and double-escape peaks of lines with energies greater than the pair production threshold. The linearity at any given channel was determined by fitting a cubic equation to the six nearest calibration energy lines.

The relative efficiency curve was obtained by using radioactive sources with known branching ratios, whose energy ranges overlapped. As a verification of the results a set of absolute calibration sources were run with a known geometry.

A. Isotope Corrections

Once the energies corresponding to peaks in the various spectra had been evaluated they were corrected for isotopic impurities to convert them to energies of the principal isotope. In the cases of ^{120}Sn, ^{138}Ba, and ^{140}Ce the targets were of high enough purity (~98% monoisotopically pure) that the measured energies could be assigned directly to the transition energies in these targets. In ^{142}Ce and ^{206}Pb the isotopic impurities were sufficiently large that a correction was applied for isotope shifts. For the K lines this was relatively easy since transitions from different isotopes were resolved and since the splittings have been measured accurately in other experiments.[37-39] The $^{140-142}$Ce K-isotope shift was measured directly and will be discussed with the results. When the lines of interest had not been studied before and could not be resolved, a different technique was required. In order to calculate the splittings, the Dirac equation was solved numerically using approximate, but reasonable values for the nuclear charge parameters, until a correct K isotope splitting was predicted. The isotope shifts of the other levels were then evaluated from these two solutions.

If $\bar{x}$ is the measured center of the peak and x is

the actual center then

$$\bar{x} = (1-\alpha)x + \alpha(x+\delta) = x + \alpha\delta \ , \qquad (4)$$

where α is the fractional impurity and δ is the isotope shift for the level in question. Since $\alpha < 0.1$ the only states to which a correction was necessary were the $1s$, $2s$, $2p_{1/2}$, and $2p_{3/2}$ states.

TABLE VI. Principal lines of the calibration sources used to determine energies, relative efficiences, and linearity.

Source	Reference	Energies (keV)	Purpose
^{22}Na	a	511.006(0.002)	**Gain calibration and**
		1274.53(0.10)	*L* and *M* feed through
^{46}Sc	b	889.18(0.10)	Gain calibration
		1120.41(0.10)	and *L* feed through
^{57}Co	b	121.97(0.05)	Gain calibration and
		136.33(0.04)	detector efficiency
^{88}Y	a	898.04(0.04)	Gain calibration and
		1836.13(0.04)	detector efficiency
^{192}Ir	a	5 lines between	Gain calibration and
		295 and 612 keV	detector efficiency
^{182}Ta	b	6 lines between	Gain calibration
		222 and 1221 keV	
^{110}Ag^m	c	15 lines between	Gain calibration and
		446 and 1562 keV	detector efficiency
^{54}Mn	a	834.81(0.03)	Gain calibration and
			detector efficiency
^{137}Cs	a	661.635(0.076)	Gain calibration and
			detector efficiency
^{177}Lu^m	d	13 lines between	Gain calibration and
		105 and 378 keV	detector efficiency
^{56}Co	e	846.78(0.06)	*L* and *M* feed through,
		1037.90(0.05)	gain calibration,
		1238.30(0.04)	511-keV energy
		1771.42(0.07)	differences,
		2034.92(0.07)	detector efficiency
		2598.57(0.06)	
		+9 other lines between 977 and 3450 keV	
^{198}Au	a	411.795(0.009)	Gain calibration
^{24}Na	a	2753.92(0.12)	*K* and *L* feed throughs,
		1368.526(0.044)	gain calibration, and
			511-keV differences
ThC″	a	238.624(0.009)	*K* feed through, gain
		583.139(0.023)	calibration, and
		2614.47(0.10)	detector efficiency
^{60}Co	a	1173.23(0.04)	*L* feed through, gain
		1332.49(0.04)	calibration, and
			detector efficiency
^{133}Ba	a	4 lines between	Gain calibration and
		276 and 384 keV	detector efficiency
^{66}Ga	f	4295.61(0.10)	*K* feed through, gain
		4806.58(0.20)	calibration, and
		+8 other lines between 1039 and 4461 keV	511-keV differences

[a] Reference 45.
[b] C. M. Lederer, J. M. Hollander, and I. Perlman, *Table of Isotopes* (Wiley, New York, 1967), 6th ed.
[c] G. Aubin, J. Barrette, M. Barrette, and S. Monaro, Nucl. Instrum. Methods 76, 93 (1969).
[d] A. J. Haverfield, F. M. Bernthal, and J. M. Hollander, Nucl. Phys. A94, 337 (1967).
[e] H. L. Scott and D. M. Van Patter, Phys. Rev. 184, 1111 (1969).
[f] M. E. Phelps, D. G. Sarantites, and W. G. Winn, Nucl. Phys. A149, 647 (1970); G. Holm, Ark. Fys. 37, 1 (1967).

TABLE VII. Calculated isotope shifts used for the ^{142}Ce and ^{206}Pb targets. The energies are in keV and the $3d$ levels are assumed to have zero isotope shift.

	Ce	Pb [a]	
	140–142	206–207	206–208
$1s_{1/2}$	15.4	5.0	11.6
$2s_{1/2}$	2.8	1.3	2.9
$2p_{1/2}$	0.4	1.5	2.3
$2p_{3/2}$	0.2	0.6	1.4

[a] Reference 37.

The appropriate isotope shifts are given in Table VII.

B. Nuclear Parameters

As discussed previously not all muon levels are equally sensitive to the nuclear parameters. Since the parameters are determined by a least-squares-fitting technique, the inclusion of accurately known transition energies for high n values, which are essentially pointlike, or of energies with large errors, will result in an artificially reduced value for the χ^2 test. The only transition energies or energy differences used to evaluate the nuclear parameters were those having a substantial finite-size dependence and a small error. In practice this included transition energies or differences involving the $1s$, $2s$, $2p_{1/2}$, $2p_{3/2}$, $3p_{1/2}$, and $3p_{3/2}$ states with errors less than 0.6 keV. The use of energy differences was prompted by the lack of an adequate number of calibration sources above 2 MeV for use in absolute energy determinations. However, an energy difference could still be accurately evaluated because of the independent measurements of the 511.006-keV energy differ-

TABLE VIII. Transition energies and energy differences used to derive nuclear charge parameters for each target.

	^{120}Sn	^{138}Ba	^{140}Ce	^{142}Ce	^{206}Pb
$2p_{3/2}$-$1s_{1/2}$	×	×	×	×	×
$2p_{1/2}$-$1s_{1/2}$	×	×	×	×	×
$4d_{3/2}$-$2p_{1/2}$	×	×	×	×	×
$3d_{3/2}$-$2p_{1/2}$	×	×	×	×	×
$3d_{5/2}$-$2p_{3/2}$	×	×	×	×	×
$3d_{3/2}$-$2p_{3/2}$	×	×	×	×	×
$3p_{3/2}$-$2s_{1/2}$	×	×	×	×	
$3p_{1/2}$-$2s_{1/2}$	×	×	×	×	
$2s_{1/2}$-$2p_{1/2}$	×	×	×	×	×
$2s_{1/2}$-$2p_{3/2}$	×	×	×	×	×
$2p_{3/2}$-$2p_{1/2}$ [a]	×			×	×
$3p_{3/2}$-$3d_{5/2}$ [a]					×

[a] Measured as a difference between two peaks.

ences. The $4d_{5/2} - 2p_{3/2}$ transition was excluded from the fitting procedure because of its contamination by the $4d_{3/2} - 2p_{3/2}$ transition and by the electric quadrupole transitions $4f_{7/2} - 2p_{3/2}$ and $4f_{5/2} - 2p_{3/2}$. Table VIII shows the combinations of various energies which were used to evaluate the nuclear parameters for each target.

The use of a four-parameter Fermi distribution and the inclusion of one nuclear polarization parameter (NP) gives five independent variable parameters to be extracted from the experimental data. These five parameters cannot be fitted simultaneously to the four energy levels with appreciable finite-size dependence, which we studied. To derive as much information as possible the following fits were made:

(1) Nuclear polarization was assumed zero for all the states and the transitions were fitted to a normal two-parameter Fermi distribution.

(2) The theoretical nuclear polarization correction was applied to each state and the transitions were fitted to a normal two-parameter Fermi distribution.

(3) The transitions were fitted to a normal two-parameter Fermi distribution with the $1s$ nuclear polarization permitted to vary, other levels assuming the theoretical values.

(4) When corresponding work had been done with electron scattering the experimental value of w was inserted and fits (2) and (3) repeated. In addition, fits were attempted in which w, m, and the $2s$ nuclear polarization were also allowed to vary.

The results from these latter fits (4) were insufficiently sensitive to justify applying them to all targets. Also, a considerable number of different fits had been tried with ^{208}Pb,[12(b)] and the resulting nuclear polarization parameters were very similar and essentially no sensitivity of these data to either w or m was observed.

C. Relative Intensities

Although not the primary intent of this experiment, measurements were made of the relative intensities of the various muonic transitions. The calculation of the peak areas is explained in Ref. 12(b). Since isotopic impurities should add a known fraction to each peak, and since only ratios were evaluated, no corrections were made to the relative intensities for isotope contamination.

The calibration sources and energies used to derive the relative efficiency curve are given in Table VI. The curve (Fig. 2) was extrapolated beyond 4.8 MeV by measuring the relative intensities of the K, L, and M lines for high-Z materials and comparing them with theoretical predictions. The relative efficiency corrections for members of a fine-structure multiplet were calculated by fitting the relative efficiency curve to a mathematical function,

$$\epsilon(E)/\epsilon(E_0) = (E/E_0)^c \tag{5}$$

using a least-squares-fitting technique. E_0 is some arbitrary energy chosen as a standard and c is a variable parameter.

The theoretical values of the relative intensities were calculated from a cascade program written by Hüfner.[40] We assumed an initial statistical distribution ($P_l = 2l+1$) in the $n = 14$ level, which has a radius equivalent to the first electronic Bohr orbit.

From the early stages of the analysis it became obvious that electric quadrupole transitions were being observed[41] and that the cascade program should be amended to account for these transitions, as well as for the finite-size effect of the muonic wave functions. Using the nonrelativistic long wavelength approximation the electric L-multipole transition probability $P(E_l, j \to j')$ becomes[8]

$$P(E_l, j \to j') = 2\alpha \left(\frac{mc^2}{\hbar}\right) J(jj'L) \left(\frac{\Delta E}{mc^2}\right)^{2L+1} M_L^{\,2}, \tag{6}$$

where

$$J(jj'L) = \frac{2j'+1}{(\alpha Z)^{2L}} \frac{L+1}{L(2L+1)[(2L-1)!!]^2} \begin{pmatrix} j & j' & L \\ \frac{1}{2} & -\frac{1}{2} & 0 \end{pmatrix}^2 .$$

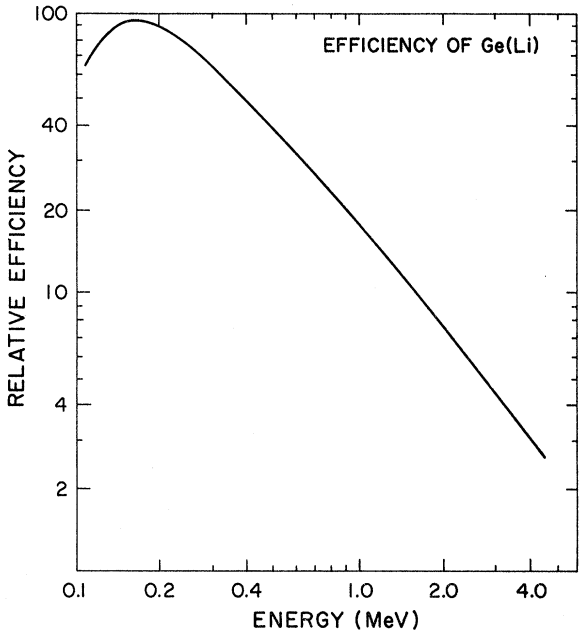

FIG. 2. Relative efficiency curve of the Ge(Li) detector in range 0.1 to 5 MeV.

The last set of parentheses represents a 3-j symbol,

$$M_L = \langle r^L \rangle = \left(\frac{Z}{a_\mu}\right)^L \int_0^\infty r^L (ff' + gg') r^2 dr,$$

and ΔE is the transition energy. The muonic Bohr radius and mass are given by a_μ and m, respectively, and f, g and f', g' are the initial and final muon radial wave functions which are obtained from the numerical solution to the Dirac equation.

To account for the effects mentioned above, point-nucleus wave functions were used in the cascade calculation only for levels $n > 4$. For $n \leq 4$ the probabilities for electric dipole and electric quadrupole transitions were calculated using Eq. (6) and the population of each lower level predicted. For muonic transitions in high-Z atoms the probability of Auger emission is extremely small for $n \leq 4$ and was neglected.

The population of each lower level as a percentage of the total number of muons captured into bound atomic states of muonic ^{140}Ce is given in Table I. The comparison between theory and experiment was used primarily as corroborative identification of the $2s$ state, but was also very useful in the identification and analysis of the electric quadrupole transitions.

4. RESULTS

A. General Procedure

The presentation of the results will be in the form of separate sections for each target analyzed, with an additional section summarizing the results on nuclear polarization. The section on each target will contain details of the specific calibrations used, a complete listing of the x rays observed, including energies and intensities, and a summary and comparison of the various sets of nuclear parameters derived. The χ^2 per degree of freedom is calculated for each set and is used to compare the relative merits of the fits. In the determination of energies, particular care was taken in evaluating those transition energies which were used to derive nuclear parameters. This meant using several alternative methods for determining gains and absolute energies. The energies of other peaks were evaluated by only one method and were hence assigned larger errors. A weighted average is quoted for some of the higher transitions in which the spectral line consists of two or more unresolved components. The averaging included all components which contributed more than 10% of the intensity, and each component was weighted according to its theoretical relative intensity. In the text and figures these averages will be denoted by the principal quantum numbers of the energy levels involved; that is all unresolved $n = 6$ to $n = 4$ transitions are denoted "6–4."

In many cases spectral lines were detected whose origins were unknown, but whose energies were accurately measured. When these appear in a figure they are described solely by their energy.

In order to detect the $3p$-$2s$ and $2s$-$2p$ transition doublets it was necessary to have a large-volume detector, with good resolution, as well as a relatively pure and intense muon beam. The choice of targets was governed by the desirability of clean single peaks, with a minimum of isotopic contamination and no hyperfine structure. As a means of positive identification of a transition involving the muonic $2s$ state, the following conditions were required:

(1) Good agreement between the experimentally measured energy and the theoretical value obtained by using the best available nuclear parameters. The validity of the parameters was checked by comparing the energies of the easily identified lines.

(2) The splitting of the fine-structure components of the two doublets should be in agreement with the fine-structure splitting measured from other transitions. The $2s$-$2p$ splitting was readily compared with the $2p$-$1s$ splitting. The $3p$-$2s$ splitting was compared to the $3p$-$1s$ splitting whenever possible, but was not as positive a test since the latter transitions were contaminated by the $3d$-$1s$ electric quadrupole transitions and were often statistically limited.

(3) Approximate agreement between the theoretical and experimental values of both the absolute and relative intensities of the fine-structure components.

(4) The absence of γ-ray peaks at the same energy in the delayed spectrum indicating that the event was truly prompt.

Each of the four transitions involving the muonic $2s$ state was unambiguously detected for ^{120}Sn, ^{138}Ba, ^{140}Ce, and ^{142}Ce. For ^{206}Pb three of the transitions were detected but there was some ambiguity with one of them.

Excluding ^{206}Pb, the relative-intensity measurements in each target were measured with respect to the $3d_{3/2}$ - $2p_{1/2}$ transition which was assigned its theoretical value. This transition was used since it is an intense single line and its energy lies between those of the lower transitions and the $2p$-$1s$ lines. For ^{206}Pb the $4f_{5/2}$ - $3d_{3/2}$ transition was used since it is the closest principal transition to the $2s$ transitions.

When relative intensities of 3-1 transitions are given they are usually quoted within the multiplet because the measurements were taken from the double-escape peaks.

TABLE IX. Energies and relative intensities of the transitions used to derive nuclear charge parameters for ^{120}Sn. A comparison is made with the theoretical predictions and other experimental results. Energies are quoted in keV, and numbers in parentheses denote uncertainties.

Levels	Energy (keV)	Other experiment	Theory [a]	Relative intensity	Theoretical relative intensity
$2p_{3/2}$-$2p_{1/2}$	45.60(0.15)	45.8(0.2) [b]	45.73		
$2p_{3/2}$-$1s_{1/2}$	3454.41(0.33)	3454.5(0.5) [b]	3453.26	50.8(8.2)	59.70
		3446.4(6.4) [c]			
$2p_{1/2}$-$1s_{1/2}$	3408.79(0.37)	3408.7(0.5) [b]	3407.54	28.0(4.5)	31.04
$4d_{3/2}$-$2p_{1/2}$	1369.50(0.26)		1369.44	2.7(0.5)	2.54
$3d_{3/2}$-$2p_{1/2}$	1022.20(0.20)	1022.6(3.0) [d]	1022.16	25.05 [e]	25.05
$3d_{5/2}$-$2p_{3/2}$	982.20(0.20)	982.5(3.0) [d]	982.41	44.7(7.0)	43.91
$3d_{3/2}$-$2p_{3/2}$	976.55(0.30)		976.43	5.0(1.12)	4.72
$3p_{3/2}$-$2s_{1/2}$	747.15(0.35)		746.26	0.82(0.5)	0.76
$3p_{1/2}$-$2s_{1/2}$	733.20(0.35)		733.51	1.1(0.3)	0.49
$2s_{1/2}$-$2p_{1/2}$	280.14(0.45)		280.02	1.29(0.4)	0.98
$2s_{1/2}$-$2p_{3/2}$	234.50(0.30)		234.29	1.51(0.34)	1.22

[a] Calculated with parameters: c = 1.1040 fm, t = 2.362 fm, *N.P.* $1s$ = 5.8 keV.
[b] Reference 42.
[c] Reference 43.
[d] Reference 44.
[e] Used as a relative intensity standard.

B. ^{120}Sn Nucleus

The 10 transition energies and the one energy difference used to derive nuclear charge parameters are given in Table IX, together with theoretical values, previous experimental values, and theoretical and experimental relative intensities.

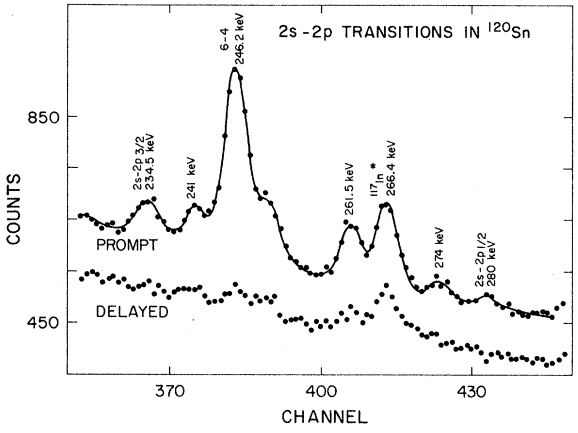

FIG. 3. Region of $2s$-$2p$ transitions in ^{120}Sn. Gain was 0.683 keV per channel and both transitions were detected. Five additional peaks were measured and two were identified as the 6-4 muonic x-ray transition at 246.2 keV and a nuclear γ ray from ^{117}In at 266.4 keV. The latter is probably a transition between the lowest $3/2^-$ and $1/2^-$ states. See C. M. Lederer, J. M. Hollander, and I. Perlman, *Table of Isotopes* (Wiley, New York, 1967), 6th ed.

A precise comparison can only be made with the work of Ehrlich,[42] since the other numbers were deduced for natural Sn.[43,44] Full details of the other transitions which were detected and identified are given in Table X.

The $2p_{3/2}$-$2p_{1/2}$ energy difference given in Table IX was evaluated from the K lines. In addition to its sensitivity to the nuclear parameters this value is important since it determines the exact energy splitting of the $2s$-$2p$ doublet. Three independent measurements were made of this quantity. The double- and single-escape peaks and photopeaks of the K lines were used to give a

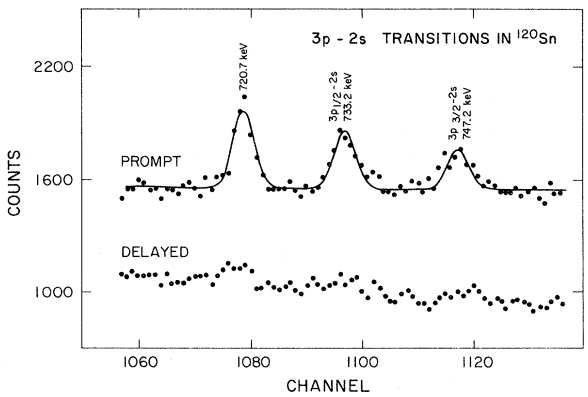

FIG. 4. Region of $3p$-$2s$ transitions in ^{120}Sn. No identification was made of the peak at 720.7 keV.

TABLE X. Other transitions observed in ^{120}Sn.

Levels	Energy (keV)	Average theoretical energy	Theoretical [a] energy	Relative intensity	Theoretical relative intensity
$5d_{3/2}$-$2p_{1/2}$	1529.14(0.8)		1530.03	0.8(0.4)	0.59
$5d_{5/2}$-$2p_{3/2}$	1484.9(0.7)	1485.48	1485.59	1.26(0.3)	1.05
$5d_{3/2}$-$2p_{3/2}$			1484.30		0.10
$4f_{7/2}$-$2p_{3/2}$			1327.66		0.37
$4d_{5/2}$-$2p_{3/2}$	1325.9(0.5)	1326.11	1326.23	4.0(0.7)	4.32
$4d_{3/2}$-$2p_{3/2}$			1323.71		0.45
$7d_{5/2}$-$3p_{3/2}$			643.66		0.13
$7f_{7/2}$-$3d_{5/2}$	642.50(0.7)	642.47	642.06	0.5(0.2)	0.85
$6f_{5/2}$-$3d_{3/2}$	595.82(0.7)		595.75	1.3(0.3)	0.7
$6f_{7/2}$-$3d_{5/2}$	590.22(0.6)		590.14	1.32(0.3)	1.0
$5f_{7/2}$-$3d_{5/2}$	504.30(0.6)		503.92	4.8(0.8)	4.78
$4f_{5/2}$-$3d_{3/2}$	350.0(0.3)		349.98	23.1(3.8)	22.86
$4f_{7/2}$-$3d_{5/2}$	345.3(0.3)		345.25	40.34(7.0)	32.24
$6f_{5/2}$-$4d_{3/2}$			248.48		0.72
$6f_{7/2}$-$4d_{5/2}$	246.21(0.6)	245.91	246.32	8.7(1.5)	1.01
$6g_{7/2}$-$4f_{5/2}$			246.21		3.44
$6g_{9/2}$-$4f_{7/2}$			245.18		4.46

[a] Calculated with parameters: $c = 1.040$ fm, $t = 2.362$ fm, *N.P.* $1s = 5.8$ keV.

weighted average. The absolute energy values of the K lines were evaluated using ThC'' and ^{24}Na calibration sources feeding through into the spectrum in accidental coincidences with stopping muons. Both these sources have an intense line which falls between the single- and double-escape peaks of the K lines. The energies of the K lines were then accurately evaluated by using these energy standards and by determining the gain from either a ^{56}Co source, or from the 511-keV energy differences.

The energies of the $3d$-$2p$, or L lines, were determined using both ^{46}Sc and ^{56}Co calibration sources in "feed-through" runs. Both these sources have γ-ray energies which closely bracket the L lines and in addition the ^{56}Co has higher energy lines which were used to evaluate the $4d$-$2p$ energies. The four lines involving the muonic $2s$ state were evaluated by determining the gain with ^{133}Ba, ^{192}Ir, and ^{22}Na calibration sources, and then relating them to either the 511-keV position annihilation peak, or one of the L lines in the summed spectrum. The $2s$-$2p$ region of the spectrum is shown in Fig. 3 and the $3p$-$2s$ region is shown in Fig. 4. Peak identifications are shown wherever possible. The $2s$-$2p$ lines were identified by their absolute energies, their energy splitting, and their relative intensity. The identification of the $3p$-$2s$ lines appears fairly conclusive but there were two ambiguities. The first was their anomalous intensities, and the second was the presence of a peak at 720.7 keV, whose origin is unknown and which was predominantly of prompt character. All three peaks had contamination from small peaks in the delayed spectrum, but even when these were allowed for, the intensities were higher than predicted theoretically. It is unfortunate that additional identification could not be obtained on the energy splitting from the 3-1 transitions, but insufficient data were obtained to give reliable fits.

Since no parallel work had been done with electron scattering, all the fits to nuclear charge parameters assumed zero central depression, and were restricted to two-parameter Fermi charge distributions. The results of the fits are summa-

TABLE XI. Nuclear charge parameters for ^{120}Sn.

Type	*N.P.* $1s$ (keV)	c (fm)	t (fm)	w	χ^2/degrees of freedom
Fermi	5.8(1.5)	1.1040(0.0091)	2.362(0.10)	0 [a]	10.7/8
Fermi	0 [a]	1.1186(0.0074)	2.154(0.092)	0 [a]	11.6/9
Fermi	2.7 [a]	1.1073(0.0089)	2.305(0.10)	0 [a]	16.9/9

[a] Held constant during fitting procedure.

TABLE XII. Energies and relative intensities of the transitions used to derive nuclear charge parameters for ^{138}Ba. A comparison is made with the theoretical predictions and other experimental results. Energies are quoted in keV, and numbers in parentheses denote uncertainties.

Levels	Energies (keV)	Other experiment [a]	Theory [b]	Relative intensity	Theoretical relative intensity
$2p_{3/2}$-$1s_{1/2}$	3988.09(0.27)	3988.26(0.40)	3988.01	65.0(10.0)	59.76
$2p_{1/2}$-$1s_{1/2}$	3922.15(0.30)	3922.25(0.40)	3922.15	31.0(6.0)	31.23
$4d_{3/2}$-$2p_{1/2}$	1720.40(0.30)		1720.60	2.0(0.4)	2.32
$3d_{3/2}$-$2p_{1/2}$	1283.22(0.12)	1283.46(0.28)	1283.35	25.65 [c]	25.65
$3d_{5/2}$-$2p_{3/2}$	1227.09(0.15)	1227.28(0.28)	1226.99	47.0(6.0)	45.06
$3d_{3/2}$-$2p_{3/2}$	1218.03(0.23)	1217.44(0.9)	1217.49	5.3(0.8)	4.70
$3p_{3/2}$-$2s_{1/2}$	886.50(0.30)		886.55	1.1(0.3)	0.83
$3p_{1/2}$-$2s_{1/2}$	868.10(0.30)		868.48	0.49(0.13)	0.44
$2s_{1/2}$-$2p_{1/2}$	405.41(0.25)		405.54	1.10(0.25)	0.91
$2s_{1/2}$-$2p_{3/2}$	339.50(0.30)		339.68	1.27(0.25)	1.15

[a] Reference 39.
[b] Calculated with parameters: $c = 1.1152$ fm, $t = 2.226$ fm, *N.P.* $1s = 6.7$ keV.
[c] Used as a standard.

TABLE XIII. Other transitions observed in ^{138}Ba.

Levels	Energy (keV)	Average theoretical energy	Theoretical energy [a]	Relative intensity [b]	Theoretical relative intensity
$3d_{5/2}$-$1s_{1/2}$	5215.3(1.0)	5214.48	5215.00	2.3(1.0) [c]	1.26
$3p_{3/2}$-$1s_{1/2}$			5214.23		2.64
$3p_{1/2}$-$1s_{1/2}$	5196.7(1.0)		5196.17	1.1 [c]	1.15
$5d_{5/2}$-$2p_{3/2}$	1859.0(0.7)		1858.94	2.74(0.5)	1.05
$4f_{7/2}$-$2p_{3/2}$			1660.90		0.54
$4d_{5/2}$-$2p_{3/2}$	1658.31(0.5)		1658.71	4.8(0.9)	4.03
$4d_{3/2}$-$2p_{3/2}$		1658.63	1654.74		0.40
$6f_{5/2}$-$3d_{3/2}$	749.6(0.7)		750.26	1.13(0.3)	1.04
$6d_{5/2}$-$3p_{3/2}$	741.10(0.5)	741.35	741.43	0.56(0.22)	0.17
$6f_{7/2}$-$3d_{5/2}$			741.34		1.48
$5f_{5/2}$-$3d_{3/2}$	641.3(0.5)		641.57	2.9(0.5)	3.36
$5f_{7/2}$-$3d_{5/2}$	632.96(0.45)		633.08	5.0(0.8)	4.78
$5d_{5/2}$-$3p_{3/2}$		630.05	632.72		0.43
$4f_{5/2}$-$3d_{3/2}$	441.28(0.15)		441.44	23.8(4.0)	24.88
$4f_{7/2}$-$3d_{5/2}$			433.90		35.33
$4d_{5/2}$-$3p_{3/2}$	433.72(0.15)	433.63	432.48	37.0(8.0)	1.43
$4f_{5/2}$-$3d_{5/2}$			431.93		1.69
$8f_{7/2}$-$4d_{5/2}$			417.02		0.20
$8g_{7/2}$-$4f_{5/2}$	416.71(0.7)	416.09	416.92	1.03(0.4)	0.43
$8g_{9/2}$-$4f_{7/2}$			415.10		0.55
$7f_{5/2}$-$4d_{3/2}$			378.43		0.30
$7f_{7/2}$-$4d_{5/2}$	373.97(0.5)	374.23	374.83	2.7(0.5)	0.43
$7g_{7/2}$-$4f_{5/2}$			374.66		1.20
$7g_{9/2}$-$4f_{7/2}$			372.91		1.55
$6f_{7/2}$-$4d_{5/2}$			309.63		1.02
$6g_{7/2}$-$4f_{5/2}$	308.83(0.45)	308.71	309.50	8.33(1.2)	3.33
$6g_{9/2}$-$4f_{7/2}$			307.88		4.30
$5f_{7/2}$-$4d_{5/2}$			201.36		2.86
$5g_{7/2}$-$4f_{5/2}$	200.53(0.40)	200.55	201.27	51.0(7.0)	18.50
$5g_{9/2}$-$4f_{7/2}$			199.90		23.95

[a] Calculated with parameters: $c = 1.1152$ fm, $t = 2.226$ fm, *N.P.* $1s = 6.7$ keV.
[b] Measured with respect to the $3d_{3/2}$-$2p_{1/2}$ line.
[c] Relative intensities measured within multiplet.

TABLE XIV. Nuclear charge parameters for ^{138}Ba.

Type	*N.P.* 1*s* (keV)	*c* (fm)	*t* (fm)	*w*	χ^2/degrees of freedom
Fermi	6.7(1.4)	1.1152(0.0039)	2.226(0.051)	0 [a]	6.23/7
Fermi	0 [a]	1.1237(0.0032)	2.071(0.045)	0 [a]	13.7/8
Fermi	3.4 [a]	1.1159(0.0039)	2.200(0.051)	0 [a]	12.4/8
Fermi	6.6(1.4)	1.0641(0.0043)	2.312(0.042)	0.375 [a]	6.21/7
Electron scattering [b]		1.033	2.30	0.375	
Thompson [c]	3.4	1.122(0.011)	2.11(0.15)		

[a] Held constant during fitting procedure.
[b] Reference 46, $m=2$.
[c] Reference 39.

rized in Table XI. It can be seen that any of these fits adequately describe the experimental data. The description of the nucleus including nuclear polarization is satisfactory, and presumably more reasonable, since nuclear polarization seems clearly present at higher Z, and is predicted to increase the binding energy of the 1*s* state by 5.8 keV in Sn. The associated uncertainty is 1.5 keV and is dominated by the sensitivity of the parameters to the value assigned to the 2*s* nuclear polarization. There is a considerable variation in the nuclear parameters obtained with and without nuclear polarization, so that an improvement in the energy determination, especially for the K and L lines, together with results from electron scattering, should determine whether the nuclear polarization effect is in agreement with the theoretical predictions.

C. ^{138}Ba Nucleus

The transitions measured and identified in ^{138}Ba are shown in Tables XII and XIII. The first table consists of transitions which possess a strong dependence upon the finite nuclear size, and which were used to derive the nuclear parameters. The second table lists the other transitions detected. These were not used to derive nuclear parameters because they either had negligible dependence upon the charge parameters, or the energy uncertainty was too large, or they were members of an unresolved multiplet.

The energies of the K-line double-escape peaks were evaluated from a feed-through run using a ^{24}Na calibration source which has an intense line at 2.75 MeV known to ±120 eV (Ref. 45).

The ^{24}Na feed-through run was also used to determine the L-line energies since there is an additional calibration line at 1368 keV. A further feed-through run was taken using ^{60}Co which has γ-ray energies closely bracketing the ^{138}Ba L lines. There is excellent agreement between the energies evaluated by the Carnegie-Mellon group,[39] and by this work.

The other transitions in Table XIII were evaluated using the gain curve and relating to either the 511-keV line or the L lines. There is very little structure in the region of the 3*p*-2*s* lines and they were easily distinguished. The $8d_{3/2}$-$3p_{1/2}$ line is energy degenerate with the $3p_{1/2}$-2*s* transition, but a theoretical cascade calculation showed its intensity to be negligible. As further identification of the 3*p*-2*s* lines there is excellent agreement between the 3*p* energy splitting evaluated from this doublet and from the 3*p*-1*s* transitions. The identification of the 2*s*-2*p* transitions relied more heavily upon the energy splitting and the relative intensities, since there were many peaks in that region. The spectrum is shown in Fig. 5 with identification of the peaks wherever possible.

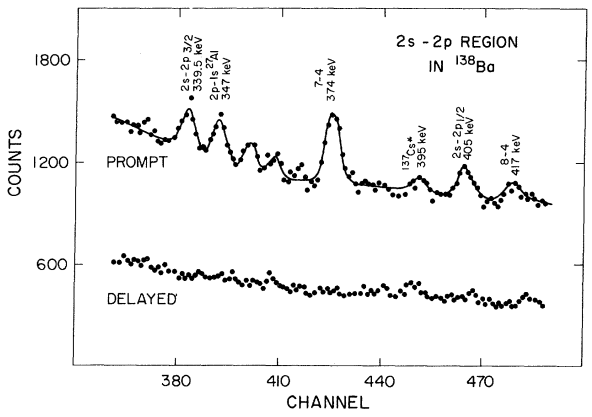

FIG. 5. 2*s*-2*p* region in ^{138}Ba. In addition to the 2*s*-2*p* doublet, six other lines were measured. Identifications were assigned to lines at 346.9 ± 0.5, 373.9 ± 0.5, 394.6 ± 0.8, and 416.9 ± 0.8 keV. The initial line is probably muonic x rays from the supporting frame or the detector cap, which are in accidental coincidence with stopping muons.

The energies of the 3-1 double-escape peaks were measured using the 511-keV difference gain curve and the K-line photopeaks. Their relative intensities do not suggest a strong contribution from electric quadrupole transitions for this low Z, but this is not entirely clear since there were insufficient data to fit the energy-separated $3d_{3/2}$-$1s$ peak at 5205 keV. The 4-2 transitions do not provide additional information on $E2$ yields since the $E2$ are energy degenerate with the $E1$ and the experimental relative intensity has a large uncertainty.

The 10 transitions identified in Table XII were fitted to several forms of charge distribution. The most successful fits were obtained using a Fermi distribution, with $m=1$.

Following Heisenberg *et al.*,[46] a sinusoidal variation was added to the Fermi distribution, but using the amplitude they suggest, the energy levels were essentially independent of this form of perturbation. The results obtained for the charge parameters are summarized in Table XIV. Using the χ^2 per degree of freedom as a measure of the goodness of fit, one finds the best agreement between theory and experiment by including nuclear polarization effects, and by allowing the $1s$ polarization to vary. Consistently the value obtained for the nuclear polarization increases the binding energy of the $1s$ state by 6.7 keV. The associated error was 1.4 keV. This is only in moderate agreement with the prediction of 3.4 ± 1.0 keV of Chen.[47] It is interesting that the same polarization result was obtained whether or not a central depression was included, although a realistic value of the central depression could not be derived from the muonic x-ray energies. The standard central depression used in these calculations for ^{138}Ba was $w=0.375$, as derived by Heisenberg *et al.*[46] from electron scattering using an $m=2$ Fermi distribution.

Table XIV gives a comparison of the ^{138}Ba charge parameters obtained from electron scattering, from Thompson's work at Carnegie-Mellon, and from this work. There is good agreement among the results.

D. ^{140}Ce Nucleus

The 10 transition energies used to derive nuclear parameters are given in Table XV. Other transitions observed and identified are shown in Table XVI.

The K-line ($2p$-$1s$) energies were measured with respect to the ^{24}Na 2.7-MeV line, which was accumulated in accidental coincidence with muon stops, and with respect to ^{56}Co and ^{66}Ga lines which were accumulated with no gating requirement. The energies of the 3-1 double-escape peaks were determined using the 2-1 photopeak energies and the gain from the 511-keV difference. These in turn were used to determine the 4-1 energies. The L lines were evaluated using a "feed-through" run with ^{22}Na and ^{60}Co calibration sources. These sources have well determined γ rays bracketing the lower L lines and were within 50 keV of the upper line. The other five principal transition energies were evaluated using a gain curve determined by calibration sources, and relating them to either the 511-keV positron annihilation line or to an L line. There was good agreement between the energies obtained in this

TABLE XV. Energies and relative intensities of the transitions used to derive nuclear charge parameters for ^{140}Ce. A comparison is made with the theoretical predictions and other experimental results. Energies are quoted in keV, and numbers in parentheses denote uncertainties.

Levels	Energy (keV)	Other experiment [a]	Theory [b]	Relative intensity	Theoretical relative intensity
$2p_{3/2}$-$1s_{1/2}$	4171.24(0.11)	4171.21(0.30)	4171.23	67.5(12.0)	59.76
$2p_{1/2}$-$1s_{1/2}$	4097.61(0.13)	4097.68(0.30)	4097.62	33.3(8.0)	31.23
$4d_{3/2}$-$2p_{1/2}$	1846.23(0.30)		1846.06	2.42(0.6)	2.32
$3d_{3/2}$-$2p_{1/2}$	1376.41(0.09)	1376.40(0.20)	1376.45	25.65 [c]	25.65
$3d_{5/2}$-$2p_{3/2}$	1313.63(0.08)	1313.70(0.20)	1313.77	42.9(6.0)	45.06
$3d_{3/2}$-$2p_{3/2}$	1303.14(0.25)	1303.34(0.50)	1302.84	4.42(0.8)	4.70
$3p_{3/2}$-$2s_{1/2}$	935.97(0.45)		935.92	1.27(0.6)	0.83
$3p_{1/2}$-$2s_{1/2}$	915.92(0.22)		915.82	0.50(0.15)	0.44
$2s_{1/2}$-$2p_{1/2}$	451.22(0.20)		451.36	0.80(0.17)	0.91
$2s_{1/2}$-$2p_{3/2}$	377.84(0.14)		377.74	1.30(0.22)	1.15

[a] Reference 39.

[b] Calculated with parameters: $c=1.1128$ fm, $t=2.313$ fm, *N.P.* $1s=6.5$ keV.

[c] Used as a standard.

experiment and those obtained at Carnegie-Mellon.[39]

The relative intensities of the 4-1 transitions are quoted within the multiplet since only the double-escape peaks had reasonable statistics. The 3-1 relative intensities were measured with respect to the $3d_{3/2}$-$2p_{1/2}$ line, but no value is quoted for the $3d_{3/2}$-$1s$ electric quadrupole transition since the photopeak had insufficient data. Electric quadrupole transitions appear important for this high value of Z, since it is only by including them that good agreement is achieved between theoretical and experimental spectra.

The identification of the $3p$-$2s$ doublet was relatively easy since there was no structure in the delayed spectrum, there was good agreement with initial energy predictions, and the $3p$ splitting could be compared to that obtained from the $3p$-$1s$ doublet.

TABLE XVI. Other transitions observed in ^{140}Ce.

Levels	Energy (keV)	Average theoretical energy	Theoretical energy [a]	Relative intensity [b]	Theoretical relative intensity
$4d_{5/2}$-$1s_{1/2}$	5948.0(1.5)	5948.38	5948.25	0.66 [c]	0.18
$4p_{3/2}$-$1s_{1/2}$			5948.42		0.50
$4p_{1/2}$-$1s_{1/2}$	5940.3(1.5)		5940.22	0.25 [c]	0.25
$3d_{5/2}$-$1s_{1/2}$	5484.54(0.5)		5485.01	4.8(1.3)	1.26
$3p_{3/2}$-$1s_{1/2}$		5484.94	5484.90		2.64
$3d_{3/2}$-$1s_{1/2}$	5474.0(0.8)		5474.08	•••	0.79
$3p_{1/2}$-$1s_{1/2}$	5464.2(0.7)		5464.81	1.6(0.5)	1.15
$6d_{5/2}$-$2p_{3/2}$	2107.6(0.6)		2108.60	0.76(0.28)	0.45
$5d_{5/2}$-$2p_{3/2}$	1992.0(0.4)		1991.92	0.85(0.25)	1.05
$4f_{7/2}$-$2p_{3/2}$			1779.51		0.54
$4d_{5/2}$-$2p_{3/2}$	1777.22(0.24)		1777.01	3.7(0.6)	4.03
$4d_{3/2}$-$2p_{3/2}$		1776.91	1772.44		0.40
$7f_{7/2}$-$3d_{5/2}$			865.57		0.70
$7f_{5/2}$-$3d_{5/2}$	865.34(0.30)		865.14	0.69(0.3)	0.49
$7d_{5/2}$-$3p_{3/2}$		865.38	865.22		0.10
$6f_{5/2}$-$3d_{3/2}$	805.58(0.30)		805.86	0.9(0.2)	1.04
$6f_{7/2}$-$3d_{5/2}$	795.49(0.30)	795.53	795.60	3.83(0.6)	1.48
$6f_{5/2}$-$3d_{5/2}$			794.93		0.17
$5f_{5/2}$-$3d_{3/2}$	688.96(0.20)		689.20	2.4(0.4)	3.36
$5f_{7/2}$-$3d_{5/2}$	679.12(0.20)		679.43	4.1(0.6)	4.78
$4f_{5/2}$-$3d_{3/2}$	474.35(0.15)		474.40	21.5(3.0)	24.88
$4f_{7/2}$-$3d_{5/2}$	465.63(0.15)		465.73	32.2(4.0)	35.33
$8f_{7/2}$-$4d_{5/2}$			447.60		0.20
$8g_{7/2}$-$4f_{5/2}$	446.90(0.25)	446.54	447.50	2.26(0.26)	0.43
$8g_{9/2}$-$4f_{7/2}$			445.40		0.55
$7f_{5/2}$-$4d_{3/2}$	406.1(0.4)		406.47	0.4(0.15)	0.30
$7f_{7/2}$-$4d_{5/2}$			402.32		0.43
$7g_{7/2}$-$4f_{5/2}$	401.42(0.20)		402.15	2.41(0.35)	1.20
$7g_{9/2}$-$4f_{7/2}$		401.19	400.14		1.55
$6f_{7/2}$-$4d_{5/2}$			332.36		1.02
$6g_{9/2}$-$4f_{7/2}$	331.25(0.20)		330.36	7.1(0.9)	4.30
$6g_{7/2}$-$4f_{5/2}$		331.32	332.23		3.33
$5f_{7/2}$-$4d_{5/2}$			216.19		2.86
$5g_{7/2}$-$4f_{5/2}$	215.20(0.25)		216.10	41.3(5.0)	18.50
$5g_{9/2}$-$4f_{7/2}$		215.27	214.52		23.95
$8f_{7/2}$-$5d_{5/2}$			232.69		0.12
$8g_{7/2}$-$5d_{5/2}$			232.82		0.35
$8g_{9/2}$-$5f_{7/2}$	231.13(0.30)	231.67	231.70	2.77(0.37)	0.48
$8h_{9/2}$-$5g_{7/2}$			231.65		0.71
$8h_{11/2}$-$5g_{9/2}$			231.07		0.88
$7g_{7/2}$-$5f_{5/2}$			187.35		1.04
$7g_{9/2}$-$5f_{7/2}$	186.2(0.35)	186.34	186.44	7.6(1.0)	1.36
$7h_{9/2}$-$5f_{7/2}$			186.52		2.86
$7h_{11/2}$-$5g_{9/2}$			185.86		3.50

[a] Calculated with parameters: $c = 1.1128$ fm, $t = 2.313$ fm, *N.P.* $1s = 6.5$ keV.

[b] Measured with respect to the $3d_{3/2}$-$2p_{1/2}$ transition.

[c] Relative intensity measured within the multiplet.

The region of the $2s$-$2p$ transitions in ^{140}Ce is shown in Fig. 6. The $2s$-$2p$ identification was complicated since the upper line was almost coincident with a peak at 447 keV, which appeared in both prompt and delayed spectra. This line was identified as a combination of the 8-4 muonic x-ray lines in ^{140}Ce and a μ-capture γ ray in ^{137}La (446 → 0). A third peak in that vicinity at 438 keV is most likely another delayed γ ray in ^{137}La (446 → 10). The detector resolution permitted partial separation of the upper two lines and a successful fit was made to three Gaussians.

The charge parameters were derived for a three-parameter Fermi distribution. In an earlier analysis[12(a)] a fit was made with a variable central depression w. Poor sensitivity to a central depression was indicated by the results obtained, $w = 9 \pm 7$. The fits were made with $w = 0$ and the results are shown in Table XVII. The best fit was obtained by allowing nuclear polarization to vary, although a satisfactory fit was obtained with zero nuclear polarization. The value predicted for nuclear polarization is 6.5 ± 1.3 keV which is somewhat higher than the theoretical value of 3.6 ± 1.0 keV.[47] There is good agreement with the parameters derived by Thompson,[39] who used the theoretical value for nuclear polarization. Our parameter uncertainties are smaller because of the additional transitions used to derive the parameters.

E. ^{142}Ce Nucleus

Since there was a 7% contamination of ^{140}Ce in the ^{142}Ce target, most peaks in the spectra had two unresolved components, one from ^{140}Ce and one from ^{142}Ce. Energy corrections were applied for this using Eq. (4) and the isotope shifts in Table VII. This amounted to 2.8 keV for the $2s$ level and was negligible (<0.05 keV) for levels with $n \geq 3$. No correction was needed for the K lines since the two components were clearly resolved. The transitions detected and identified are listed in Tables XVIII and XIX. Table XVIII contains the energies used in determining nuclear parameters, and, in addition to the usual transitions, it includes the $2p$ doublet splitting as determined from the K lines. This was included because of the relatively large errors on the K lines.

Making use of the observed isotope splitting the $2p$-$1s$ energies have been determined from the corresponding lines in ^{140}Ce. In making these energy measurements, accurate values were obtained for the $2p$ splitting, and for 140-142 isotope shift (S_I) of the two K lines. The latter values are

$$S_I(2p_{3/2} - 1s) = 15.38 \pm 0.30 \text{ keV},$$

$$S_I(2p_{1/2} - 1s) = 14.80 \pm 0.29 \text{ keV},$$

where the higher energies belong to ^{140}Ce. For these, and the absolute K-line energies, there is moderately good agreement with the work of Thompson.[39]

To evaluate the L lines a feed-through run was taken using ^{60}Co and ^{22}Na calibration sources. The region of interest is shown in Fig. 7. The accuracy of the calibration lines and their proximity to the lines of interest enabled very accurate energy determinations to be made. The other five principal transitions were evaluated by relating them to either the 511-keV line, an L line, or an M line.

The identification of both $2s$-$2p$ and $3p$-$2s$ doublets was complicated by the presence of other

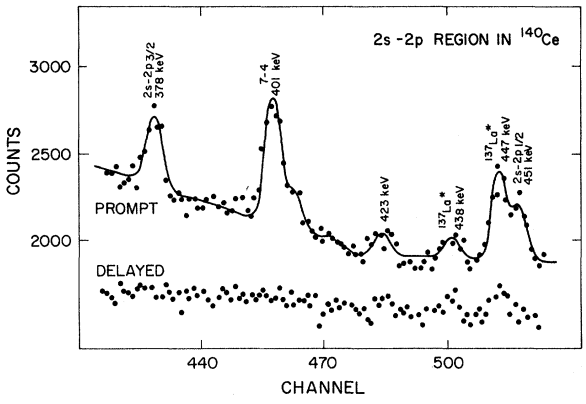

FIG. 6. Spectra in the region of the $2s$-$2p$ doublet in ^{140}Ce. The $2s$-$2p_{1/2}$ line is contaminated by two γ rays at 446.9 ± 0.4 and 438.0 ± 1.0 keV. These have been identified as probable transitions in ^{137}La, 446→0 and 446→10, respectively. [See C. M. Lederer, J. M. Hollander, and I. Perlman, *Table of Isotopes* (Wiley, New York, 1967), 6th ed.] Gain is 0.805 keV per channel.

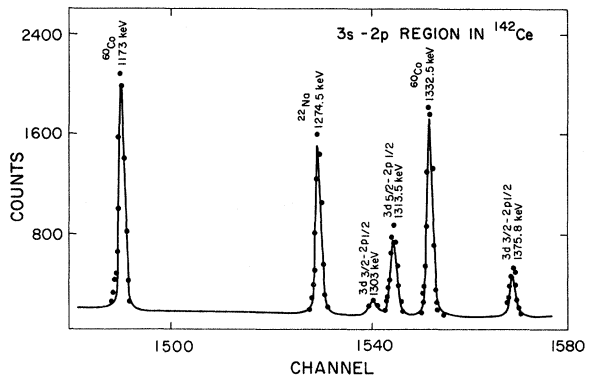

FIG. 7. Evaluation of ^{142}Ce L lines using ^{22}Na and ^{60}Co calibration source in accidental coincidence with muon stops. Gain is 0.805 keV per channel.

TABLE XVII. Nuclear charge parameters for ^{140}Ce.

Type	*N.P.* 1*s* (keV)	*c* (fm)	*t* (fm)	*w*	χ^2/degrees of freedom
Fermi	6.5(1.3)	1.1128(0.0032)	2.313(0.042)	0 [a]	2.45/7
Fermi	0 [a]	1.123 18(0.0023)	2.140(0.031)	0 [a]	9.06/8
Fermi	3.6 [a]	1.1148(0.0030)	2.276(0.039)	0 [a]	7.64/8

[a] Held constant during fitting procedure.

peaks in the region of interest. The spectrum near the $2s$-$2p$ doublet is shown in Fig. 8. The lower line, $2s$-$2p_{3/2}$, has a small background peak appearing in the spectrum near the same energy. To account for this, it was assumed that the prompt-to-delayed area ratio was the same for the delayed peak under the $2s$-$2p_{3/2}$, as for the adjacent γ ray at 389 keV. This fraction of the delayed peak at 380 keV was then subtracted from the prompt peak and the intensity error increased proportionately. The upper line, $2s$-$2p_{1/2}$, was overlapped by the muonic 8-4 transitions, as well as being on the lower edge of the very intense $4f_{7/2}$-$3d_{5/2}$ line. In the figure the 4-3 transitions are omitted since they far exceed the scale used. Fits were taken of two Gaussians on an exponential background, as well as three and four Gaussians, the latter including both 4-3 transitions. The peak center remained consistent within the fitted errors, and the mean center was used with a slightly enlarged error.

The $3p$-$2s$ region is shown in Fig. 9. The $3p$-$2s$ peaks were positively identified from approximate energy, energy splitting, and relative intensity. The peak directly above the doublet corresponds in energy to the lower-energy members of the 9-3 transitions. Its intensity is substantially larger than anticipated from a simple cascade calculation, and it is also surprising that no other peaks appear below and between the $3p$-$2s$ lines, which would correspond to 8-3 transitions. Note that the 7-3 transitions appear clearly in the lower part of the spectrum.

The energy values of the 3-1 transitions were determined from the $2p$-$1s$ photopeak energies using a 511-keV energy difference.

The energies were fitted to Fermi distributions and the results are summarized in Table XX. The most satisfactory fit was obtained using a variable nuclear polarization in the $1s$ state which gave a value of 7.0 ± 1.4 keV. This is higher than the theoretical nuclear polarization of 3.6 keV,[47] although a 25% decrease in the polarization effect on the $2s$ level produces better agreement between the two polarization values. Fits were also attempted using a variable central depression. These gave a central depression which was indistinguishable from zero.

TABLE XVIII. Energies and relative intensities of the transitions used to derive nuclear charge parameters for ^{142}Ce. A comparison is made with the theoretical predictions and other experimental results. Energies are quoted in keV, and numbers in parentheses denote uncertainties.

Levels	Energy (keV)	Other experiment [a]	Theory [b]	Relative intensity	Theoretical relative intensity
$2p_{3/2}$-$2p_{1/2}$	73.07(0.09)		73.30		
$2p_{3/2}$-$1s_{1/2}$	4155.86(0.32)	4156.21(0.50)	4155.93	70.0(12.0)	59.76
$2p_{1/2}$-$1s_{1/2}$	4082.81(0.32)	4083.3(0.50)	4082.63	37.7(10.0)	31.23
$4d_{3/2}$-$2p_{1/2}$	1846.10(0.50)		1845.46	2.40(0.5)	2.32
$3d_{3/2}$-$2p_{1/2}$	1375.80(0.10)		1375.85	25.65 [c]	25.65
$3d_{5/2}$-$2p_{3/2}$	1313.47(0.08)		1313.48	48.0(8.0)	45.06
$3d_{3/2}$-$2p_{3/2}$	1303.10(0.25)		1302.55	5.9(1.2)	4.70
$3p_{3/2}$-$2s_{1/2}$	932.55(0.38)		933.16	1.08(0.3)	0.83
$3p_{1/2}$-$2s_{1/2}$	913.00(0.30)		913.17	0.50(0.13)	0.44
$2s_{1/2}$-$2p_{1/2}$	453.45(0.40)		453.63	1.50(0.40)	0.91
$2s_{1/2}$-$2p_{3/2}$	379.90(0.25)		380.33	1.40(0.50)	1.15

[a] Reference 39.

[b] Calculated with parameters: $c = 1.1258$ fm, $t = 2.181$ fm, *N.P.* $1s = 7.0$ keV.

[c] Used as a standard.

TABLE XIX. Other transitions observed in ^{142}Ce.

Levels	Energy (keV)	Average theoretical energy	Theoretical energy [a]	Relative intensity	Theoretical relative intensity
$3d_{5/2}$-$1s_{1/2}$	5469.6(0.6)	5469.42	5469.41	3.0 [b]	1.26
$3p_{3/2}$-$1s_{1/2}$			5469.43		2.64
$3d_{3/2}$-$1s_{1/2}$	5459.7(1.0)		5458.48	0.58 [b]	0.79
$3p_{1/2}$-$1s_{1/2}$	5449.2(0.5)		5449.43	1.15 [b]	1.15
$5d_{3/2}$-$2p_{1/2}$	2062.42(0.8)		2062.60	0.69(0.26)	0.59
$5d_{5/2}$-$2p_{3/2}$	1993.14(0.8)	1991.44	1991.64	1.61(0.47)	1.05
$5d_{3/2}$-$2p_{3/2}$			1989.30		0.10
$4f_{7/2}$-$2p_{3/2}$			1779.22		0.54
$4d_{5/2}$-$2p_{3/2}$	1777.27(0.5)	1776.69	1776.73	4.64(0.8)	4.03
$4d_{3/2}$-$2p_{3/2}$			1772.16		0.40
$9f_{7/2}$-$3d_{5/2}$	942.20(0.6)	941.97	942.01	1.0(0.2)	0.25
$9d_{5/2}$-$3p_{3/2}$			941.76		0.05
$7f_{5/2}$-$3d_{3/2}$	876.10(0.5)		876.09	1.1(0.2)	0.49
$7f_{7/2}$-$3d_{5/2}$			865.58		0.70
$7f_{5/2}$-$3d_{5/2}$	866.03(0.5)	865.38	865.16	1.09(0.2)	0.49
$7d_{5/2}$-$3p_{3/2}$			865.11		0.10
$6f_{5/2}$-$3d_{3/2}$	804.97(0.7)		805.88	0.85(0.2)	1.04
$6f_{7/2}$-$3d_{5/2}$	794.84(0.6)	795.54	795.61	1.42(0.3)	1.48
$6f_{5/2}$-$3d_{5/2}$			794.94		0.17
$5f_{5/2}$-$3d_{3/2}$	688.64(0.5)		689.21	3.39(0.5)	3.36
$5f_{7/2}$-$3d_{5/2}$	679.14(0.45)	679.33	679.44	4.99(0.7)	4.78
$5d_{5/2}$-$3p_{3/2}$			678.14		0.43
$4f_{5/2}$-$3d_{3/2}$	474.24(0.20)		474.41	24.4(3.5)	24.88
$4f_{7/2}$-$3d_{5/2}$	465.46(0.20)		465.74	36.2(5.0)	35.33
$7f_{7/2}$-$4d_{5/2}$			402.33		0.43
$7g_{7/2}$-$4f_{5/2}$	401.07(0.5)	401.20	402.16	3.4(0.5)	1.20
$7g_{9/2}$-$4f_{7/2}$			400.14		1.55
$6f_{7/2}$-$4d_{5/2}$			332.36		1.02
$6g_{7/2}$-$4f_{5/2}$	331.20(0.45)	331.32	332.24	8.5(1.2)	3.33
$6g_{9/2}$-$4f_{7/2}$			330.37		4.30
$8f_{7/2}$-$4d_{5/2}$			447.60		0.20
$8g_{7/2}$-$4f_{5/2}$	447.3(0.5)	446.55	447.51	1.0(0.4)	0.43
$8g_{9/2}$-$4f_{7/2}$			445.41		0.55
$5f_{7/2}$-$4d_{5/2}$			216.19		2.86
$5g_{7/2}$-$4f_{5/2}$	215.01(0.4)	215.28	216.10	51.6(7.0)	18.50
$5g_{9/2}$-$4f_{7/2}$			214.53		23.95

[a] Calculated with parameters: $c = 1.1258$ fm, $t = 2.181$ fm, *N.P.* $1s = 7.0$ keV.
[b] Relative intensities calculated within the multiplet.

TABLE XX. Nuclear charge parameters for ^{142}Ce.

Type	*N.P.* $1s$ (keV)	c (fm)	t (fm)	w	χ^2/degrees of freedom
Fermi	7.0(1.4)	1.1258(0.0034)	2.181(0.048)	0 [a]	14.6/8
Fermi	0 [a]	1.1334(0.0030)	2.035(0.046)	0 [a]	31.2/9
Fermi	3.6 [a]	1.1262(0.0034)	2.160(0.047)	0 [a]	20.7/9

[a] Held constant during fitting procedure.

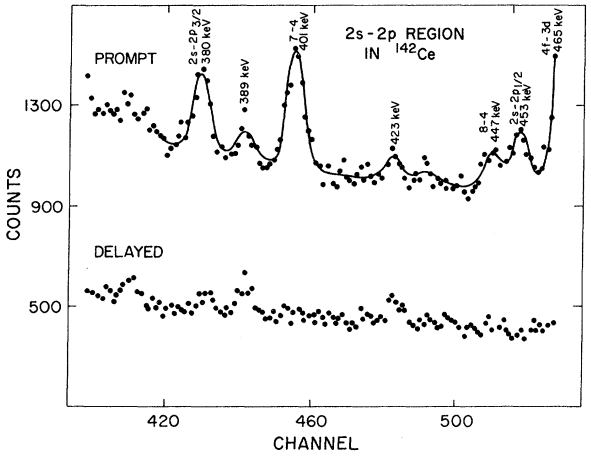

FIG. 8. Spectrum in the region of the $2s$-$2p$ doublet in ^{142}Ce. Both $2s$-$2p$ peaks are contaminated with other lines. The upper falls on the edge of the very intense $4f_{7/2}$-$3d_{5/2}$ peak as well as overlapping a small prompt peak, which is probably the muonic 8-4 transition. The lower-energy peak has some structure under it in the delayed spectrum but by comparing with the adjacent γ ray at 389.8 ± 0.5 keV (origin unknown), it is clear this effect is small.

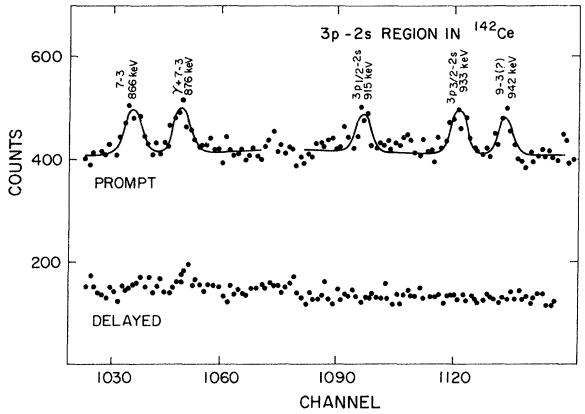

FIG. 9. Spectrum in the region of the $3p$-$2s$ doublet in ^{142}Ce. Also fitted were the 7-3 transitions and a peak at 942.0 ± 0.7 keV which corresponds in energy to the 9-3 transitions but is much more intense than theoretical predictions.

F. ^{206}Pb Nucleus

The principal transitions and energy differences which have been accurately determined in ^{206}Pb are shown in Tables XXI and XXII. Table XXI shows those transitions which were used to derive nuclear parameters. Table XXII contains the other principal transitions and energy differences which were measured and identified. Two fine-structure splittings were used to help derive the nuclear parameters since the K lines had relatively large errors and since no other transitions which involved the $3p$ states were positively identified. The $3p$-$1s$ transitions were excluded because of their large energy uncertainties.

Because of the isotopic contamination of the target (see Table V) it was necessary to apply energy corrections to the deduced energies following Eq. (4). The isotope shifts are given in Table VII, and were either deduced from theoretical predictions or taken from the work of Anderson *et al.*[37] Since the work of Anderson *et al.* on ^{206}Pb was similar to this work a com-

TABLE XXI. Energies and relative intensities of the transitions used to derive nuclear charge parameters for ^{206}Pb. A comparison is made with the theoretical predictions and other experimental results. Energies are quoted in keV, and numbers in parentheses denote uncertainties.

Levels	Energy (keV)	Other experiments [a]	Theory [b]	Relative intensity [c]	Theoretical relative intensity
$2p_{3/2}$-$2p_{1/2}$	185.5(0.15)	185.65(0.12)	185.70		
$3p_{3/2}$-$3d_{5/2}$	37.47(0.45)		38.28		
$2p_{3/2}$-$1s_{1/2}$	5973.6(0.5)	5974.0(0.4)	5974.20	45.6(15.0)	56.28
$2p_{1/2}$-$1s_{1/2}$	5788.0(0.5)	5788.3(0.5)	5788.50	27.0(8.0)	30.95
$4d_{3/2}$-$2p_{1/2}$	3599.52(0.45)	•••	3599.01	0.9(0.3)	1.80
$3d_{3/2}$-$2p_{1/2}$	2644.50(0.40)	2643.8(0.4)	2644.50	27.3(6.0)	25.5
$3d_{5/2}$-$2p_{3/2}$	2501.60(0.20)	2501.5(0.4)	2501.68	44.8(8.0)	45.0
$3d_{3/2}$-$2p_{3/2}$	2458.85(0.60)	2458.1(0.4)	2458.80	4.5(1.0)	4.40
$2s_{1/2}$-$2p_{1/2}$	1214.84(0.50)	1217.8(0.8)	1214.85	0.6(0.18)	0.69
$2s_{1/2}$-$2p_{3/2}$	1029.03(0.45)	•••	1029.15	0.55(0.17)	0.92

[a] Reference 37.
[b] Calculated with parameters: $c = 1.1215$ fm, $t = 2.324$ fm, $N.P.$ $1s = 5.5$ keV.
[c] Measured with respect to the $4f_{5/2}$-$3d_{3/2}$ transition.

TABLE XXII. Other transitions observed in ^{206}Pb.

Levels	Energy (keV)	Other experiments [a]	Theoretical energy [b]	Relative intensity	Theoretical relative intensity
$3d_{5/2}$-$3d_{3/2}$	43.01(0.41)		42.89		
$3p_{3/2}$-$3p_{1/2}$	47.73(1.10)		47.70		
$3p_{3/2}$-$1s_{1/2}$	8512.7(2.5)		8513.63	1.0 [c]	1.0 [d]
$3d_{5/2}$-$1s_{1/2}$	8475.3(2.4)		8475.36	1.53(0.18) [c]	1.69
$3p_{1/2}$-$1s_{1/2}$	8466.5(2.5)		8465.93	0.39(0.08) [c]	0.45
$3d_{3/2}$-$1s_{1/2}$	8432.3(2.4)		8432.47	1.18(0.14) [c]	1.03
$4f_{5/2}$-$2p_{1/2}$	3617.0(0.8)		3616.46	0.32(0.11)	0.71
$4f_{7/2}$-$2p_{3/2}$	3440.00(0.5)		3439.96	1.16(0.3)	1.40
$4f_{5/2}$-$2p_{3/2}$	3431.35(0.45)	3429.5(1.4)	3430.75	2.1(0.5)	0.20
$4d_{5/2}$-$2p_{3/2}$			3431.08		3.00
$6f_{5/2}$-$3d_{3/2}$	1640.2(1.0)		1639.83	0.53(0.19)	1.04
$6f_{7/2}$-$3d_{5/2}$	1599.6(0.7)	1598.2(1.0)	1599.67	1.17(0.27)	1.48
$3p_{3/2}$-$2s_{1/2}$	1508.8(1.5)	1507.9(0.8)	1510.81	0.84(0.5)	0.88
$5f_{5/2}$-$3d_{3/2}$	1405.2(0.6)	1404.1(0.4)	1404.65	2.53(0.6)	2.90
$5f_{7/2}$-$3d_{5/2}$	1366.75(0.6)	1366.0(0.5)	1366.49	3.95(0.7)	4.10
$4f_{5/2}$-$3d_{3/2}$	971.9(0.3)	971.7(0.2)	971.96	28.9 [d]	28.9
$4f_{7/2}$-$3d_{5/2}$	937.9(0.3)	937.8(0.2)	938.28	41.8(7.0)	39.3
$4f_{5/2}$-$3d_{5/2}$	929.6(0.5)	928.2(0.5)	929.07	3.1(0.8)	1.70
$4d_{5/2}$-$3p_{3/2}$	892.6(0.6)		891.12	0.71(0.2)	1.43
$6g_{7/2}$-$4f_{5/2}$	671.5(0.6)	670.9(0.4)	670.82	3.3(0.6)	3.33
$6f_{7/2}$-$4d_{5/2}$			670.28		1.02
$6g_{9/2}$-$4f_{7/2}$	664.0(0.6)	663.1(0.4)	663.23	4.2(0.8)	4.30

[a] Experimental result of Anderson, Ref. 37.
[b] Calculated with parameters: $c = 1.1215$ fm, $t = 2.324$ fm, *N.P.* $1s = 5.5$ keV.
[c] Relative intensity measured within multiplet.
[d] Used as a standard.

parison is made with their experimental results whenever possible.

To evaluate the K lines the ^{142}Ce target was also placed in the muon beam so that there was a well-known muonic x-ray line at 4.15 MeV for evaluating the energies of the K double-escape peaks. The 3-1 energies were then deduced from the 2-1 energies using a gain curve determined by the 511-keV energy differences. The determination of detector efficiency at this high an energy is a major problem, but since this was a secondary consideration of the experiment the relative efficiency of the detector was determined up to 3.4 MeV using a ^{56}Co source and then extrapolated linearly on a log-log plot. From experimental and theoretical comparisons at higher energies, it appears that the detector efficiency decreased faster than the extrapolated predictions. Because of this uncertainty in detector efficiency, the relative intensities of the 3-1 energy transitions at 8.4 MeV are only quoted relative to each other.

A ^{56}Co calibration source was run under accidental gating conditions to determine energies of the L and M lines. In addition to bracketing both of these lines it was used to determine the gain and the relative efficiency. Using this gain the $2s$-$2p$ lines were evaluated using both the M lines and the double escape of the L lines as energy standards, while the 4-2 lines were related to the L-line photopeaks.

The analysis of the transitions involving the $2s$ states is complicated by the presence of structure in both the prompt and delayed spectra. Figure 10 shows the prompt and delayed spectra in the region of $2s$-$2p_{3/2}$ with the Gaussians fitted in both spectra superimposed. The three Gaussians fitted in the prompt spectrum correspond to transitions with energies of 1029, 1038, and 1043 keV, respectively. Peaks were fitted in the delayed spectrum with energies of 1038 and 1043 keV. The prompt-to-delayed ratios of the 1038 and 1043 peaks were consistent with their identification as delayed γ rays. These γ rays were tentatively identified as transitions in the Ge detector, ^{70}Ge (1040 → 0) and in ^{205}Pb (1044 → 0). The remaining peak at 1029.0 ± 0.45 keV was then identified as the $2s$-$2p_{3/2}$ transition. Although its intensity is less than anticipated, it is consistent with similar results obtained in ^{208}Pb.[12(b)]

The $2s$-$2p_{1/2}$ region is shown in Fig. 11. The initial analysis of the prompt and delayed spectra were in terms of four Gaussians and the resultant areas suggested that there was some prompt contribution to the central peak. However the width

of the prompt peaks was anomalously large and the fit was relatively poor, so that the prompt spectrum was reanalyzed in terms of five Gaussians, the central peak being assumed a doublet. This resulted in an improved fit, a width consistent with other adjacent peaks, and better agreement with the peaks fitted in the delayed spectrum. The peaks common to the prompt and delayed spectra have been identified as being at 1208, 1219, 1227, and 1234 keV, whereas the remaining prompt line is at 1214.8 ± 0.5 keV and is identified as the $2s$-$2p_{1/2}$ transition. Its intensity is in poor agreement with theory but again is consistent with results obtained in ^{208}Pb.[12(b)] A further fact supporting both $2s$-$2p$ identifications is the $2p$ doublet splitting, which is in excellent agreement with that determined from the K lines. In the previous four-Gaussian fit this energy splitting was inconsistent, but the absolute $2s$-$2p_{1/2}$ energy agreed with the earliest results of Anderson *et al.*,[37] who also obtained a value of 1217.8 keV, but were unable to detect the lower $2s$-$2p_{3/2}$ transition.

No peak could be identified in the spectrum which would correspond with the $3p_{1/2}$-$2s$ transition. A peak was found corresponding to the $3p_{3/2}$-$2s$ transition, but it was wider than expected, and a small peak was found in the delayed spectrum, which could be contributing to this anomalous width. It was possible to fit the prompt peak with two Gaussians, but neither corresponded well with the peak in the delayed spectrum. Because of the large uncertainty in the energy of the $3p_{3/2}$-$2s$ peak, and because its relative intensity was substantially below the theoretical predictions, and the results obtained in ^{208}Pb, it was omitted from the nuclear parameter analysis.

To compensate for the lack of these two transitions, which involved the useful $3p$ states, an energy difference involving the $3p_{3/2}$ state was included in the nuclear parameter analysis. This was evaluated from the 3-1 transitions using the 511-keV energy differences. In ^{206}Pb the $3d$-$1s$ electric quadrupole transitions are clearly separated from the $3p$-$1s$ electric dipole transitions as shown in Fig. 12. Although the quadrupole-transition rate is relatively weak, the $3d$-$1s$ transitions have intensity comparable to the $3p$-$1s$ transition because of the greater population of the initial state. The energy dependence is clearly evident in a comparison to the 4-2 transitions, where the $4f$-$2p$ quadrupole-transition intensities are less than half those of the $4d$-$2p$ dipole intensities. There is good agreement between theoretical and experimental energy differences adding credence to the calculations by Skardhamar,[6] which indicates a substantial nuclear polarization effect in the $3p$ states. Had this not been included, the $3p_{3/2}$-$3d_{5/2}$ energy difference would have been two standard deviations away from the theoretical predictions. All the high-energy relative intensities are lower than predicted but this can probably be attributed to detector-efficiency uncertainties. A comparison of quadrupole-to-dipole relative intensities within a multiplet which should be approximately independent of detector efficiency, shows them to be in good agreement with theoretical predictions.

The results of nuclear parameter fits are shown

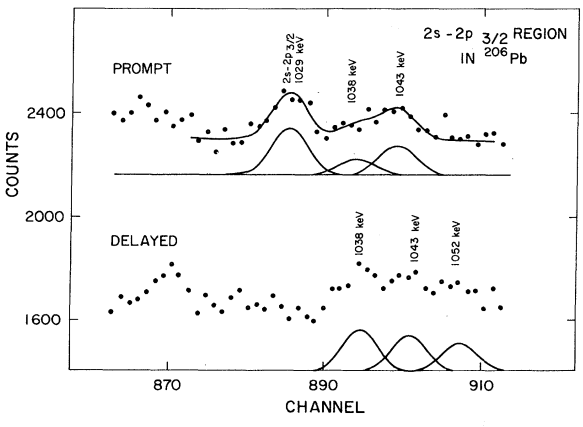

FIG. 10. Spectra in the region of the $2s$-$2p_{3/2}$ transition in ^{206}Pb. The Gaussians fitted in the prompt and delayed spectra are indicated. The prompt peaks at 1038.0 ± 1.0 and 1043.2 ± 0.8 keV also appear in the delayed spectrum, and the peak at 1029 keV is identified as $2s$-$2p_{3/2}$. The γ rays were tentatively identified as coming from ^{70}Ge (1040→0) and ^{205}Pb (1044→0).

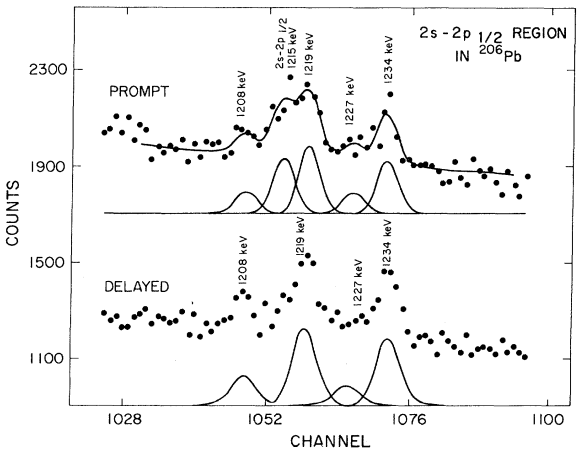

FIG. 11. Spectra in the region of the $2s$-$2p_{1/2}$ transition in ^{206}Pb. The Gaussians fitted in the prompt and delayed spectra are superimposed but with false zero levels. The unidentified peaks which appeared in both prompt and delayed spectra were at 1207.6 ± 0.8, 1219.1 ± 0.5, 1227.0 ± 1.5, and 1234.0 ± 1.5, and 1234.0 ± 0.7 keV. The gain was 1.1 keV per channel.

in Table XXIII. It was found that no useful information could be derived by allowing the central depression to vary, so fits were done with either $w = 0$, or with $w = 0.14$, the value inferred from electron scattering.[25] The χ^2 per degree of freedom for the fits with nuclear polarization, and with or without a central depression, are extremely low. Since a value of 1 is accepted as a good fit it seems that several of the assigned energy errors are overly conservative. However, there is evidence that the inclusion of nuclear polarization produces far better agreement between theory and experiment than when it is omitted. When treated as a variable parameter it converges to a value of 5.5 ± 1.7 keV if one uses the theoretical values of Chen for the $2s$ and $2p$ levels and 6.7 ± 2.2 keV if one uses the values of Skardhamar. Essentially the same value is obtained when a central depression is included, and both are in excellent agreement with the predictions of Chen[5] and Skardhamar.[6] A further fit was obtained by allowing the nuclear polarization effect on the $2s$ level to be treated as a variable. This again produced a good fit, but the large errors are to be expected since only two transitions involving the $2s$ state were included. When compared to the nuclear parameters of Anderson *et al.*[37] there is poor agreement, which may be attributed to the fact that the fitting conditions are not the same. Anderson *et al.* did not use a variable nuclear polarization, nor did they apply nuclear polarization corrections to the higher levels. In an analysis of more recent data[48] they have applied these corrections and there is much better agreement between the two sets of parameters. A fit with $m = 2$ which changes the falloff of the charge distribution produced a nuclear polarization value consistent with the other fits.

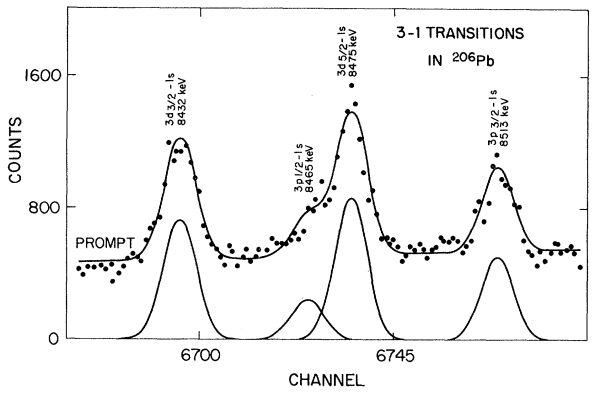

FIG. 12. Prompt spectrum for the 3-1 transitions in ^{206}Pb. The $3d$-$1s$ lines are quadrupole transitions. The delayed spectrum has no structure. The gain is 1.1 keV per channel.

G. Summary of Results

So far the results from each target have been discussed independently. The purpose of the set of experiments was to investigate the general behavior of nuclear polarization in comparison with theoretical predictions, and this will be considered now. The results obtained with ^{208}Pb [Ref. 12(b)] will also be considered, since they made up part of this set of experiments and were analyzed in a similar fashion. Direct comparisons between the theoretical and experimental results, are made in Table XXIV and Fig. 13. The experimental values obtained seemed independent of the form of the charge distribution used, and to the presence or absence of a central depression. This last statement should be qualified in that only Fermi-like distributions were used.

TABLE XXIII. Nuclear charge parameters for ^{206}Pb.

Type	*N.P.* 1*s* (keV)	*N.P.* 2*s* (keV)	*c* (fm)	*t* (fm)	*w*	χ^2/degrees of freedom
Fermi [a]	5.5(1.7)	1.2 [b]	1.1215(0.0015)	2.324(0.021)	0 [b]	4.89/7
	6.7(2.8)	1.6 [b]	1.1236(0.0026)	2.294(0.036)	0 [b]	8.23/7
Fermi	0 [b]	0 [b]	1.1280(0.0011)	2.194(0.018)	0 [b]	14.4/8
Fermi [a]	5.4(1.7)	1.2 [b]	1.0997(0.0015)	2.399(0.019)	0.14 [b]	4.90/7
	6.6(2.8)	1.6 [b]	1.1019(0.0026)	2.371(0.032)	0.14 [b]	8.41/7
Fermi [a]	9.2(4.7)	2.3(1.3)	1.126 04(0.0055)	2.264(0.074)	0 [b]	4.65/6
	7.9(5.2)	2.0(1.5)	1.1252(0.0061)	2.273(0.083)	0 [b]	8.56/6
Fermi ($m = 2$)	5.7(1.7)	1.2 [b]	1.1120(0.0018)	12.342(0.059)	0 [b]	5.08/7
Fermi [c]	0 [b]	0 [b]	1.133(0.004)	2.102(0.079)		

[a] The upper numbers were obtained using the Chen values for the nuclear polarization and theoretical uncertainty, the lower numbers used the Skardhamar values.

[b] Held constant during fitting procedure.

[c] Reference 37.

TABLE XXIV. Comparison of theoretical and experimental nuclear polarization values. With the exception of ^{208}Pb the experimental values were derived from fits to the experimental energies using three variable parameters.

	^{120}Sn	^{138}Ba	^{140}Ce	^{142}Ce	^{206}Pb	^{208}Pb
Cole	1.6	2.0	2.2		5.3	
Chen	2.7(1.0)	3.4(1.0)	3.6(1.0)		6.0(0.6)	
Skardhamar	•••	•••	•••		6.8(2.0)	
Experiment	5.8(1.5)	6.7(1.4)	6.5(1.3)	7.0(1.4)	5.5(1.7) [a]	12.0(1.5)
					6.7(2.8)	

[a] The upper numbers were obtained using the Chen values for the nuclear polarization and theoretical uncertainty; the lower numbers used the Skardhamar values.

It can be seen from Fig. 13 that the experimental values follow the trend of the theoretical predictions, but tend to be somewhat larger. In ^{208}Pb it was found that the value of the $2s$ nuclear polarization strongly affected the $1s$ nuclear polarization and it was hence also allowed to vary. When this was done for ^{206}Pb large errors were obtained for all the parameters. This was caused by having an insufficient number of charge-sensitive transitions with small errors.

To understand the absence of the $3p_{1/2}$-$2s$ transition in ^{206}Pb it is necessary to know what number of counts would be anticipated. By comparison with the ratio of transitions from the $3p$ states to the $1s$ state, the $3p_{1/2}$-$2s$ transition would have a maximum amplitude of 70 counts on a background of 1700, and would be barely detectable. These numbers assume a 30% γ-ray contamination of the prompt $3p_{3/2}$-$2s$ peak. Because of the difficulty of estimating detector efficiencies at 8.5 MeV the relative intensities of the 3-1 transitions are measured within the multiplet, and no correlation can be made with the relative intensities of other transitions. From our problem in detecting the $3p$-$2s$ peak it appears that the $3p$ states may be preferentially depopulated. A possible explanation of this may be the proposal by Srinivasan and Sundaresan,[49] that a muonic np state ($n \geq 3$) may deexcite 60% of the time by the emission of a prompt neutron leaving the muon in the $1s$ state and hence reducing the number of radiative transitions from the np states.

5. CONCLUSIONS

Because of the good agreement between theory and experiment for the lead isotopes, when nuclear polarization is included, it appears that nuclear polarization is a relatively important correction to the nuclear parameters of high-Z nuclei. It also appears to give better fits in the region of $Z = 58$, although the improvement of fit is not so dramatic.

A measurement of a single isotope or the constraint of a charge-parameter fit to theoretical nuclear polarization values may give fits which do not unambiguously give evidence for nuclear polarization. However, in the range of isotopes measured here, the fit to charge parameters consistently seemed to require a nuclear polarization to agree with the data in higher-Z elements.

Assuming that it is necessary for the higher-Z elements, then it should also be applicable to the lower-Z elements, and if one is to determine the nuclear charge parameters, then nuclear polarization effects should be included. The results of this work do not give definitive values for nuclear polarization effects in all targets, but they do indicate that the calculations of Chen[5] and Skardhamar[6] are more consistent with experimental results, than the predictions of Cole.[4] In order to reduce the uncertainty in the interpretation of the $1s$ level, it will be necessary to improve the theoretical uncertainty in the Lamb shift, at present estimated at 30%.

In addition to further calculations of the Lamb shift, more theoretical work on the nuclear polarization of the $3p$, $3s$, and $4s$ states would be most

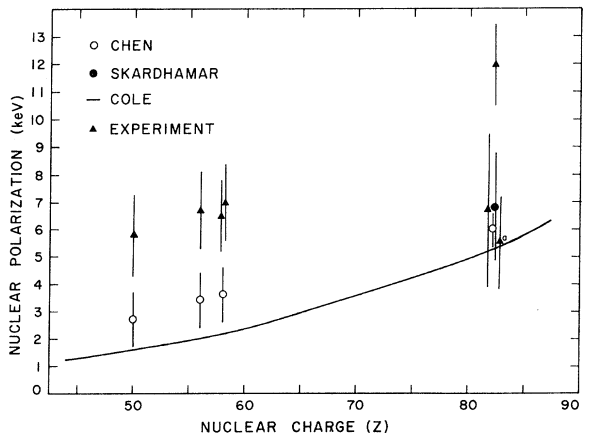

FIG. 13. Variation of nuclear polarization with Z. Wherever available, error bars have been included.

useful, since with the advent of high-efficiency detectors and contemporary data-collecting facilities, these levels will undoubtedly be important in future muonic x-ray experiments. This is especially true for the $3s$ level, since its wave-function overlap with the nucleus makes it the next most sensitive level beyond the $2s$. This may be used to provide additional information on a central depression and allow a better comparison with electron-scattering results. The central depression evaluated from electron-scattering work seems to be consistent with the muonic x-ray analysis. This fact supports the assertion of Negele[50] that the most accurate description of a nucleus can be obtained from the combination of electron-scattering and muonic x-ray work.

Future experiments should attempt to decrease the uncertainties on the energies, since it is clear that only this reduction will permit one to obtain more definitive information about the nuclear charge distribution. Transitions of particular interest in future experiments are the $3p$-$1s$ transitions, which would provide another measurement directly dependent upon the $1s$ nuclear polarization. For these transitions it will be necessary to take into account the electric quadrupole transitions, which have been shown to have comparable intensity and to be nearly energy degenerate with the $3p$-$1s$ lines.

ACKNOWLEDGMENTS

The authors would like to acknowledge the helpful discussions and suggestions of Professor D. G. Ravenhall, Professor L. Wilets, Professor D. H. Wilkinson, and Dr. Min-Yi Chen. We are grateful to Dr. R. T. Siegel and the staff of the Space Radiation Effects Laboratory for their hospitality and efficiency, and also to the William and Mary Physics Department electronics and machine shops for their construction of much of the apparatus. We appreciate the loan of the separated isotopes by Dr. G. L. Rogosa and Dr. E. Ritter.

---

*Work supported by the National Aeronautics and Space Administration, the National Science Foundation, and the Atomic Energy Commission.

†Present address: Philip Morris Research Center, Commerce Road, Richmond, Virginia.

‡Gulf Oil Corporation graduate fellow. Present address: Lawrence Livermore Laboratory, Livermore, California.

§Present address: Physics Department, California Institute of Technology, Pasadena, California 91109.

[1]J. A. Wheeler, Rev. Mod. Phys. 21, 133 (1949).

[2]J. A. Wheeler, Phys. Rev. 71, 320 (1947).

[3]D. L. Hill and K. W. Ford, Phys. Rev. 94, 1617 (1954).

[4]R. K. Cole, Jr., Phys. Lett. 25B, 178 (1967); Phys. Rev. 177, 164 (1969).

[5]M. Y. Chen, Phys. Rev. C 1, 1167 (1970).

[6]H. F. Skardhamar, Nucl. Phys. A151, 154 (1970).

[7]D. West, Rept. Prog. Phys. 21, 271 (1958).

[8]S. Devons and I. Duerdoth, Advan. Nucl. Phys. 2, 295 (1969).

[9]C. S. Wu and L. Wilets, Ann. Rev. Nucl. Sci. 19, 529 (1969).

[10]F. Scheck and J. Hüfner, to be published.

[11]D. Kessler, H. L. Anderson, M. S. Dixit, H. J. Evans, R. J. McKee, C. K. Hargrove, R. D. Barton, E. P. Hincks, and J. D. McAndrew, Phys. Rev. Lett. 18, 1179 (1967); H. L. Anderson, C. K. Hargrove, E. P. Hincks, J. D. McAndrew, R. J. McKee, and D. Kessler, Phys. Rev. Lett. 22, 221 (1969).

[12](a) D. A. Jenkins, R. J. Powers, P. Martin, G. H. Miller, R. E. Welsh, and A. R. Kunselman, Phys. Lett. 32B, 267 (1970). (b) D. A. Jenkins, R. J. Powers, P. Martin, G. H. Miller, and R. E. Welsh, Nucl. Phys. A175, 73 (1971).

[13]H. Backe *et al.*, Nucl. Phys. A189, 472 (1972).

[14]R. J. McKee, Phys. Rev. 180, 1139 (1969).

[15]K. W. Ford and J. G. Wills, LASL Report No. LA-DC-10393, 1968 (unpublished).

[16]H. Daniel, Ecole Internationale de la Physique de Particule Elementaire, Herceg-Novi, Yugoslavia, Report, 1969 (unpublished).

[17]J. A. Wheeler, Phys. Rev. 92, 812 (1953).

[18]L. N. Cooper and E. M. Henley, Phys. Rev. 92, 801 (1953).

[19]K. W. Ford and J. G. Wills, Los Alamos Scientific Report No. LAMS-2387, 1960 (unpublished).

[20]K. W. Ford and J. G. Wills, Nucl. Phys. 35, 295 (1962).

[21]R. C. Barrett, Phys. Lett. 33B, 388 (1970).

[22]F. G. Perey and J. P. Schiffer, Phys. Rev. Lett. 17, 324 (1966).

[23]L. R. B. Elton and A. Swift, Nucl. Phys. A94, 52 (1967); *Nuclear Sizes* (Oxford U. P., Cambridge, 1961).

[24]L. R. B. Elton, S. J. Webb, and R. C. Barrett, in *High Energy Physics and Nuclear Structure*, edited by S. Devons (Plenum, New York, 1970), p. 67.

[25]J. Heisenberg, R. Hofstadter, J. S. McCarthy, I. Sick, B. C. Clark, R. Herman, and D. G. Ravenhall, Phys. Rev. Lett. 23, 1402 (1969).

[26]D. Vautherin and D. M. Brink, Phys. Lett. 32B, 149 (1970).

[27]J. Schwinger, Phys. Rev. 75, 651 (1949).

[28]J. Blomquist, Nucl. Phys. B48, 95 (1972).

[29]P. Vogel, California Institute of Technology Report No. CALT-63-191 (unpublished).

[30]B. Fricke, Phys. Rev. Lett. 30, 119 (1973).

[31]M. S. Dixit, H. L. Anderson, C. K. Hargrove, R. J. McKee, D. Kessler, H. Mes, and A. C. Thompson, Phys. Rev. Lett. 27, 878 (1971).

[32]H. K. Walter, J. H. Vuilleumier, H. Backe, F. Boehm, R. Engfer, A. H. V. Gunten, R. Link, R. Michaelsen, C. Petitjean, L. Schellenberg, H. Schneuwly, W. U. Schröder, and A. Zehnder, Phys. Lett. 40B, 197 (1972).

[33]R. C. Barrett, S. J. Brodsky, G. W. Erickson, and

M. H. Goldhaber, Phys. Rev. 166, 1589 (1968).
[34]G. Breit, G. B. Arfken, and W. W. Clendenin, Phys. Rev. 78, 390 (1950).
[35]V. L. Fitch and J. Rainwater, Phys. Rev. 92, 789 (1953).
[36]K. Tanabe, Phys. Rev. A 3, 1282 (1971).
[37]H. L. Anderson, C. K. Hargrove, E. P. Hincks, J. D. McAndrew, R. J. McKee, R. D. Barton, and D. Kessler, Phys. Rev. 187, 1565 (1969).
[38]R. J. Powers, Phys. Rev. 169, 1 (1968).
[39]A. C. Thompson, thesis, Carnegie-Mellon University, 1969 (unpublished).
[40]We are greatly indebted to J. Hüfner who kindly provided us with a copy of his muon-cascade program.
[41]P. Martin, G. H. Miller, R. E. Welsh, D. A. Jenkins, and R. J. Powers, Phys. Rev. Lett. 25, 1406 (1970).
[42]R. D. Ehrlich, Phys. Rev. 173, 1088 (1968).
[43]H. L. Anderson, C. S. Johnson, and E. P. Hincks, Phys. Rev. 130, 2468 (1963).
[44]H. L. Acker, G. Backenstoss, C. Daum, J. C. Sens, and S. A. de Wit, Nucl. Phys. 87, 1 (1966).
[45]J. B. Marion, Nucl. Data A4, 301 (1968).
[46]J. Heisenberg, R. Hofstadter, J. S. McCarthy, I. Sick, M. R. Yearian, B. C. Clark, R. Herman, and D. G. Ravenhall, to be published.
[47]The theoretical values for nuclear polarization were taken from Figs. 12(a), 12(b), and 12(c), of Ref. 9.
[48]D. Kessler, invited paper, Muon Physics Conference, Fort Collins, Colorado, 1971 (unpublished).
[49]V. Srinivasan and M. K. Sundaresan, Can. J. Phys. 49, 621 (1971).
[50]J. W. Negele, Nucl. Phys. A138, 401 (1969).